White Adipose Tissue Compositional and Transcriptional Patterns with Progressive Glucose Intolerance in Persons with HIV

Authors: Samuel S. Bailin[1], Jonathan A. Kropski[2,3,4], Rama D. Gangula[5], LaToya Hannah[6], Joshua D. Simmons[5], Mona Mashayekhi[6], Fei Ye[7], Run Fan[7], Simon Mallal[1,5,8-10], Christian M. Warren[5], Spyros A. Kalams[1,5,10], Curtis L. Gabriel[11], Celestine N. Wanjalla[1,10,±*], John R. Koethe[1,3,10,±]

[1]Department of Medicine, Division of Infectious Diseases, Vanderbilt University Medical Center, Nashville, Tennessee, USA
[2]Department of Medicine, Division of Allergy and Pulmonology, Vanderbilt University Medical Center, Nashville, Tennessee, USA
[3]Veterans Affairs Tennessee Valley Healthcare System, Nashville, Tennessee, USA
[4]Deparment of Cell and Developmental Biology, Vanderbilt University, Nashville, Tennessee, USA
[5]Tennessee Center for AIDS Research, Vanderbilt University Medical Center, Nashville, Tennessee, USA
[6]Department of Medicine, Division of Diabetes, Endocrinology, and Metabolism, Vanderbilt University Medical Center, Nashville, Tennessee, USA
[7]Department of Biostatics, Vanderbilt University, Nashville, Tennessee, USA
[8]Insitute for Immunology and Infectious Diseases, Murdoch University, Perth, WA, Australia
[9]Vanderbilt Technologies for Advanced Genomics, Vanderbilt University Medical Center, Nashville, Tennessee, USA
[10]Center for Translational Immunology and Infectious Diseases, Vanderbilt University Medical Center, Nashville, Tennessee, USA
[11]Department of Medicine, Division of Gastroenterology, Hepatology, and Nutrition, Nashville, Tennessee, USA

[*]Corresponding Author: Celestine N. Wanjalla, MD, Ph.D.; Division of Infectious Diseases, Vanderbilt University Medical Center, A-2200 MCN, 1161 21st Avenue South, Nashville, Tennessee, 37232-2582. (615) 322-2035 (o), (615) 343-6160 (f), celestine.wanjalla@vumc.org

[±]These authors contributed equally

Abstract

Subcutaneous adipose tissue (SAT) is a critical regulator of systemic metabolic homeostasis. Persons with HIV (PWH) have an increased risk of metabolic diseases and significant alterations in the SAT immune environment compared with the general population. We generated a comprehensive SAT atlas to characterize cellular compositional and transcriptional changes in 59 PWH with a spectrum of metabolic health. Glucose intolerance was associated with increased lipid-associated macrophages and $CD4^+$ and $CD8^+$ T effector memory cells, and decreased perivascular macrophages. We observed a coordinated intercellular regulatory program which enriched for genes related to inflammation and lipid-processing across multiple cell types as glucose intolerance increased. Increased $CD4^+$ effector memory tissue resident cells most strongly associated with altered expression of adipocyte genes critical for lipid metabolism and cellular regulation. Many of these findings were present in a separate group of 32 diabetic HIV-negative persons, suggesting these changes are not specific to HIV.

Keywords: human immunodeficiency virus, type 2 diabetes mellitus, white adipose tissue, subcutaneous adipose tissue, single-cell RNA sequencing, immune cells

Introduction

The rising global rates of obesity and type 2 diabetes mellitus (T2DM) represent a significant public health challenge[1,2]. Persons with HIV (PWH) suffer disproportionately from cardiovascular disease, chronic kidney disease, and T2DM compared with the general population[3-6]. The higher risk of metabolic disease in PWH compared with the general population is likely multifactorial and stems from increasing age and survival with improved anti-retroviral therapies, a greater prevalence of known risk factors for metabolic disease including elevated body mass index (BMI), and HIV-specific risk factors including persistent inflammation[3,7-9]. Adipose tissue is an important regulator of glucose and lipid metabolism[10], and alterations in its cellular composition and function have been implicated in the development of metabolic diseases[11-15]. While alterations in adipose tissue are common in PWH[7], the underlying changes in subcutaneous adipose tissue (SAT) that contribute to metabolic disease in this population are poorly understood.

Despite the success of modern antiretroviral therapy (ART), virologically suppressed PWH have persistent innate and adaptive immune activation[16], as well as permanent alterations in the adipose tissue immune cell compartment[17]. In non-obese PWH, $CD8^+$ T cells accumulate in SAT in a process strikingly similar to that observed in obesity in the general population[18,19]. Additionally, SAT $CD4^+$ T cells in PWH shift towards an increased proportion of inflammatory and cytotoxic cells compared to HIV-negative individuals[20]. Many immune cell populations implicated in the perpetuation of chronic SAT inflammation in studies of HIV-negative individuals or animals are also altered in circulating immune cells in PWH[21,22]. Therefore, HIV may serve as a natural experimental model, to study exaggerated immune activation and cellular changes, which can shed light on SAT pathophysiology shared with the general population.

Recent studies in lean and obese persons in the general population have begun to unravel the complex cellular composition of adipose tissue[14,15,23,24]. However, a comprehensive assessment of the identity, polarization, and molecular programs of adipose tissue immune cells in PWH, a group at particularly high risk of metabolic disease, has not been reported.

We recruited a large cohort of PWH with a spectrum of metabolic health to elucidate the SAT cellular compositional and transcriptional regulatory framework that define metabolic disease. We used single-cell proteogenomics and generated a detailed molecular atlas of SAT from 59 PWH to characterize disease-specific changes in cellular populations and expression programs. In PWH with glucose intolerance, we found higher proportion of lipid-associated macrophage (LAM) and LAM-like macrophage populations, reduction of perivascular macrophages (PVMs), and an increase in $CD4^+$ and $CD8^+$ T effector memory (T_{EM}) populations that was independent of obesity, age, and sex. We further uncovered a multicellular transcriptional regulatory program with glucose intolerance characterized by a shift towards macrophage lipid processing phenotype, increasing cytotoxicity and IFN-γ phenotype in T cells, and genes associated with fibrosis. Finally, we showed that this regulatory pattern is conserved in diabetic HIV-negative individuals, suggesting that polarization of immune cells regulating adipose tissue inflammation is a shared feature of metabolic disease and not specific to PWH. These transcriptomic and other data are posted to a user-friendly interactive website (http://vimrg.app.vumc.org/).

Results

Cellular Composition Reflects the Complex Function of Subcutaneous Adipose Tissue

We enrolled individuals with a range of glucose intolerance to investigate the role of adipose tissue immune cells in the development of metabolic disease among PWH registered at ClinicalTrials.gov (NCT04451980) (Table 1). To determine the cell populations that characterize SAT in the context of glucose intolerance and HIV infection, we collected abdominal SAT from non-diabetic (n = 20), pre-diabetic (n = 19), and diabetic PWH (n = 20). We used the droplet-based 10X Genomics platform with cellular indexing of transcriptomes and epitopes by sequencing (CITE-seq)[25], to analyze surface phenotypes and transcriptomes (Fig.1a, Supplementary Fig. 1a, methods). After quality control filtering and harmony batch correction[26], (Supplementary Fig. 1b- 1e, Supplementary Tables 1-3), we obtained a final dataset with 177,942 cells from 59 participants (Fig. 1b, 1c**)**. Broadly, cells clustered into fibro-adipogenic, lymphoid, vascular, and myeloid clusters (Fig. 1d). Cells were annotated using genes previously identified in single-cell datasets (Supplementary Fig. 1f, Supplementary Tables 4 and 5)[15,27-30]. Importantly, we identified several immune cell types that have been associated with diabetes and obesity in prior studies, including LAMs[28,31], natural killer (NK) cells[32], gamma delta (γδ) T cells[33], and innate lymphoid cells (ILCs)[15,34]. We also identified three clusters (arterial EndoMT-like, venous EndoMT-like, and capillary EndoMT-like) expressing markers of both pericytes and endothelial cells[35]. Prediabetic participants had a greater proportion of vascular cells ($p_{adj} = 0.03$) and reduced proportion of myeloid and lymphoid cells ($p_{adj} = 0.04$, $p_{adj} = 0.02$, respectively) compared with non-diabetic participants (Fig. 1e).

We next subset on major cell populations for finer cell annotations. Adipose tissue macrophages and conventional dendritic cells (cDC) interact with adipocytes and can modulate

adipogenesis, insulin sensitivity, and tissue remodeling in the setting of obesity[28,36-39], though there are few similar data in PWH[40,41]. We identified 14 distinct cell populations from 40,585 cells in the myeloid compartment (Fig. 2a) using canonical gene markers (Fig. 2b, Supplementary Table 6). Surface-marker phenotyping by CITE-seq supported our classification of LAMs ($CD11C^+$), perivascular macrophages (PVMs) ($CD11C^-$), non-classical monocytes (nMo) ($CD16^+$), classical monocytes (cMo) ($CD14^+$), and DCs ($CD1C^+$) (Supplementary Fig. 2a). A subset of macrophages was labeled as intermediate macrophage (IM) and expressed markers of LAMs and PVMs (Supplementary Fig. 2b, Supplementary Table 7). Over-representation analysis demonstrates distinct pathways highlighting functional differences between macrophage subsets (Supplementary Fig. 2c).

Lymphoid cells also have a prominent role in shaping the immune environment of SAT and modulating local inflammation and insulin resistance[13,42-45]. HIV infection induces broad changes to circulating lymphoid cells associated with the development of insulin resistance including memory, senescent, and exhausted phenotypes[19,21,22,46]. From 28,061 lymphoid cells, we identified 16 distinct cell states in adipose tissue including $CD4^+$ & $CD8^+$ naïve (*SELL, LEF1, CCR7*), central memory (T_{CM}) (*LTB, LDHB, GPR183*), effector memory (T_{EM}) (*ALOX5AP, COTL1, CCL5*), cytotoxic (*NKG7, GNLY, PRF1*), and $CD4^+$ T_{reg} (*FOXP3, CTLA4*) cells. Additionally, we identified γδ T cells (*TRDV1, KLRC2*), MAIT cells (*CCR6, IL7R, KLRG1*), and ILCs *(XCL1, KIT, IL7R*). Several NK cell subsets were identifiable by cell-surface expression of CD16 and CD56 and included mature $CD16^+$ (*FCER1G, NKG7)*, terminally differentiated mature $CD16^+CD57^+$ (*FCGR3A, KLRD1*), and $CD56^+CD16^-$ (*XCL1, XCL2, SELL*) (Fig. 2c, 2d; Supplementary Table 6). The RNA transcriptome profiles were analyzed in parallel with CITE-seq surface marker expression of CD4, CD8, CD45RA, CD27, CD57, and CD16

(Supplementary Fig. 2d). We also separately assessed only $CD4^+$ and $CD8^+$ T cells to differentiate more finely between naïve, central memory, effector memory, and cytotoxic phenotypes (Supplementary Fig. 2E-2H, Supplementary Table 7). Cells classified as $CD4^+$ T_{EM} expressed higher levels of CD69, a marker of tissue residency (Supplementary Fig. 2f)[47]. We validated this by gating on $CD4^+$ $CD69^+$ T cells for 21 individuals and found high correlation with $CD4^+$ T_{EM} defined by scRNA-seq ($\rho = 0.71$, $p < 0.001$). These data suggest that expression of CD69 is a major driver of gene expression pattern.

We next evaluated fibro-adipogenic cell populations, as recent studies have revealed considerable heterogeneity[14,23,24,48-51] and interactions between fibro-adipogenic and immune cells can modulate adipocyte function and have an important role in the development of metabolic disease[39,52]. We identified 11 distinct cells states from 51,029 fibro-adipogenic cells (Fig. 2e, 2f; Supplementary Table 6). An interstitial fibroblast population ($PCOLCE^+$ fibroblast) that has been shown to give rise to preadipocytes expressing *SFRP2*, *DPP4*, and *PCOLCE2* is analogous to $PCOLCE^+$ fibroblasts in the dermis[53], and homologous to a population in mice[30]. A second fibroblast population has high expression of *MYOC* and *ITM2A*, which is consistent with anti-adipogenic CD142 cells that have been previously described[48]. A separate population of cells expressing *TIMP1* and *POSTN* is transcriptionally consistent with myofibroblasts. Adipose progenitor cells (PCs) were characterized by expression of *DCN*, *CLU*, *LUM*, *GSN*, and *PI16*. The preadipocyte compartment was largely differentiated by expression immediate early genes (*MYC*, *FOS*, *JUN*) and markers associated with adipogenesis and regulation of inflammation (*ZFP36*, *EGR1*, *KLF4*, *CEBPD*) (Early preadipocyte), and markers associated with extracellular matrix (ECM) (ECM-Producing preadipocytes). Preadipocytes progressively acquired higher expression of *FABP4*, *LPL*, and *CIDEC*, which are markers of lipid acquisition. Finally, we

found different vascular stromal and endothelial cells present in adipose tissue (Fig. 2g, 2h). In summary, we show a diversity of cell types present in SAT in persons with HIV that reflect the complex physiologic functions of adipose tissue.

Categorical and Continuous Measures of Glucose Intolerance are Associated with Macrophage and T Cell Polarization

Cellular compositional changes of SAT with progressive glucose intolerance likely reflect functional changes that either promote or are derived from the disease process. Several studies evaluating obesity have shown significant changes to the myeloid compartment with increasing proportion of LAMs and changes to T cell polarization. Less is known about compositional changes to the fibro-adipogenic compartment, though it is known that adipose tissue fibrosis occurs in the setting of obesity[54].

Within the macrophage compartment, IM and LAM proportions were higher in prediabetic (p_{adj} = 0.02 and p_{adj} = 0.03) and diabetic (p_{adj} = 0.02 and p_{adj} = 0.04) PWH compared with non-diabetic PWH. In contrast, PVM proportion was lower in prediabetic (p_{adj} = 0.02) and diabetic PWH (p_{adj} = 0.02) compared with non-diabetic PWH (Fig. 3a). In general, prediabetic and diabetic PWH had a shift away from classical monocyte (cMo) (p_{adj} = 0.02 & p_{adj} = 0.09, respectively) and other Mo (p_{adj} = 0.02 & p_{adj} = 0.02, respectively). Compared with non-diabetic PWH, cDC1 proportion was increased in diabetic PWH (p_{adj} = 0.04). A major strength of this large dataset over previous adipose tissue single cell studies is greater power to assess the independent contributions of important biological factors to cellular composition. We examined whether the cell types associated with glucose intolerance in group comparisons were associated with measurements of glucose intolerance (hemoglobin A1c [hba1c], fasting blood glucose

[FBG]) as a continuous measure. We used partial spearman's correlation adjusted for BMI, sex, and age, and we excluded diabetic PWH from the analysis given the effects of medication treatment on the endpoints. FBG was inversely associated with PVM proportion ($\rho = -0.61$, $p = 0.002$) while HbA1c was associated with LAM proportion ($\rho = 0.47$, $p = 0.01$) (Fig. 3b). Evaluating all myeloid cells, measures of glucose intolerance were significantly associated with LAM and IM proportions and inversely associated with monocyte cell proportions, particularly with HbA1c (Fig. 3c). Thus, there is an overall shift from primarily monocytes and PVMs towards a LAM-like phenotype with glucose intolerance, similar to findings in HIV-negative persons[15].

The lymphoid compartment had fewer differences by diabetes status. The proportion of $CD8^+$ T_{EM} was lower in non-diabetic PWH compared with prediabetic ($p_{adj} = 0.05$) but not diabetic PWH ($p_{adj} = 0.44$) (Fig. 3d). FBG but not HbA1c was significantly associated with $CD8^+$ T_{EM} ($\rho = 0.49$, $p < 0.001$) and inversely associated with $CD8^+$ naïve T cells ($\rho = -0.44$, $p = 0.01$) (Fig. 3e). Similarly, the proportion of $CD4^+$ T_{EM} was lower in non-diabetic PWH compared with prediabetic ($p_{adj} = 0.05$) but not diabetic PWH (Fig. 3f). This was mainly due to a significant decrease in $CD4^+$ naive T cells ($p_{adj} = 0.05$). As discussed in the previous section, $CD4^+$ T_{EM} cells expressed CD69. We confirmed with flow cytometry that participants with glucose intolerance had higher proportion of $CD4^+$ $CD69^+$ T cells (median percent: non-diabetic (6.4%), prediabetic (37.5%), diabetic (37.7%); $p = 0.01$). FBG was significantly associated with $CD4^+$ T_{EM} ($\rho = 0.51$, $p < 0.001$) and inversely associated with $CD4^+$ naïve T cells ($\rho = -0.63$, $p < 0.001$) (Fig. 3g). The proportion of $\gamma\delta$ T cell was increased in prediabetic ($p = 0.04$) but not diabetic PWH ($p = 0.54$), though was not significant after correction for multiple comparisons. FBG was independently associated with $\gamma\delta$ T cell ($\rho = 0.33$, $p = 0.04$) and $CD57^+$ mNK ($\rho =$

0.35, p = 0.05) proportion, but hbA1c was not (Supplementary Fig. 3a). In summary, prediabetic, but not treated diabetic PWH, have increased T_{EM} cells compared with non-diabetic PWH.

Finally, we hypothesized that the proportion of fibroblast populations would be increased with glucose intolerance. However, there was no significant associations between the proportion of fibro-adipogenic cells and continuous measures of glucose intolerance (Supplementary Fig. 3b) or by diabetes status (Supplementary Fig. 3c). While diabetic PWH had a greater proportion of venous EndoMT-like cells (p = 0.008) and intermediate capillary endothelial cells (p = 0.02), there were no significant differences after correction for multiple comparison and no association with measures of glucose intolerance (Supplementary Fig. 3d). Taken together, we show that in the context of glucose intolerance, PWH have dramatic changes in the myeloid cell compartment with a shift towards a LAM-like phenotype, as well as a shift towards T_{EM} T cells, but no significant difference in the fibro-adipogenic cell composition.

BMI is Associated with Macrophage Polarization while Sex is Associated with Fibro-Adipogenic Compositional Changes

Demographic variables can influence the adipose tissue environment[10]. Therefore, we next examined the relationship of cell composition with BMI, age, and sex. Evaluating all myeloid cells, BMI was associated with the proportion of IMs (ρ = 0.35, p = 0.01), LAMs (ρ = 0.27, p = 0.05), and Mo-Macs (ρ = 0.31, p = 0.03) (Fig. 4a). Similarly, age was associated with the proportion of LAMs (ρ = 0.31, p = 0.03). Evaluating the $CD4^+$ T cell subsets, age was inversely related to naïve (ρ = -0.34, p = 0.04) and regulatory T cells (ρ = -0.41, p = 0.02) (Fig. 4b). BMI was inversely related to $CD8^+$ T_{CM} proportion (ρ = -0.38, p = 0.01) (Fig. 4c). Finally,

age was inversely associated with the proportion of Progenitor 1 ($\rho = -0.31$, $p = 0.03$) (Fig. 4d). Other lymphoid and vascular cell proportions were associated with BMI and age (Supplementary Fig. 4a, 4b). In summary, higher BMI and to a lesser extent older age, was significantly associated with a shift towards LAM and LAM-like macrophages.

To assess the independent contributions of sex to cell proportions, we used an ordinal linear regression model adjusted for age, BMI, and diabetes status. Compared with men, women had higher proportion of PVMs ($p = 0.008$) and lower proportion of IMs ($p = 0.008$), but no significant differences in other myeloid cells (Fig. 4e and Supplementary Fig. 4c). Compared with men, women had lower proportion of $CD4^+$ cytotoxic ($p = 0.002$) and $CD8^+$ cytotoxic T cells ($p = 0.05$) (Fig. 4f, 4g). Women also had proportion difference in NK cells (Supplementary Fig. 4d). In contrast to BMI and age, female sex had a significant influence on fibro-adipogenic cell composition. Compared with men, women had higher proportion of PCOLCE+ fibroblasts ($p = 0.03$), PC 2 ($p = 0.004$), and early preadipocytes ($p = 0.003$), and lower proportion of mature preadipocytes 1 ($p < 0.001$) and 2 ($p < 0.001$) (Fig. 4h). Vascular cell populations were not associated with female sex (Supplementary Fig. 4e). The individual odds ratios (female: male) are available at (http://vimrg.app.vumc.org/). Taken together, sex appears to be a larger driver of compositional changes in the fibro-adipogenic compartment than either BMI or age. Female sex is associated with higher proportions of cell populations that are abundant in healthy adipose tissue.

Cell Proportions Associated with Glucose Intolerance are Highly Inter-Related

We next wanted to examine the inter-relatedness of cell populations associated with glucose intolerance using partial spearman's correlation, adjusted for BMI, age, sex, and diabetes

status. We hypothesized that immune cell populations associated with glucose intolerance would be related to each other and may be associated with fibrogenic cells in adipose tissue. The proportion of $CD4^+$ T_{EM} was significantly associated with the proportion of several myeloid cells including IMs ($\rho = 0.55$, $p = 0.001$), LAMs ($\rho = 0.48$, $p = 0.01$), PVMs ($\rho = 0.48$, $p = 0.006$), and Mo-Macs ($\rho = 0.66$, $p < 0.001$) and inversely associated with cMos ($\rho = -0.70$ $p < 0.001$) and other Mos ($\rho = -0.70$, $p < 0.001$) (Fig. 5a). The proportion of $CD8^+$ T_{EM} was also associated with the proportion of several myeloid cells including IMs ($\rho = 0.42$, $p = 0.01$), LAMs ($\rho = 0.46$, $p = 0.006$), PVMs ($\rho = 0.38$, $p = 0.02$), and cDC1s ($\rho = 0.45$, $p = 0.002$), and inversely associated with cMos ($\rho = -0.57$, $p < 0.001$) and other monocytes ($\rho = -0.72$, $p < 0.001$) (Fig. 5b). We next looked at the fibro-adipogenic cells. The proportion of $CD4^+$ T_{EM} was associated with the proportion of ECM-producing early preadipocytes ($\rho = 0.46$, $p = 0.005$) and myofibroblasts ($\rho = 0.35$, $p = 0.04$), and inversely associated with early preadipocytes ($\rho = -0.51$, $p = 0.006$)(Fig. 5c). The proportion of $CD8^+$ T_{EM} was similarly associated with the proportion of ECM-producing early preadipocytes ($\rho = 0.49$, $p = 0.004$) and inversely associated with early preadipocytes ($\rho = -0.49$, $p = 0.001$) (Fig. 5d). The proportion of IM was associated with the proportion of myofibroblasts ($\rho = 0.77$, $p < 0.001$) and inversely associated with PCOLCE+ fibroblasts ($\rho = -0.74$, $p < 0.001$) as well as several other cell types to a lesser degree (Fig. 5e). The proportion of LAMs was associated with myofibroblasts ($\rho = 0.33$, $p = 0.04$) and inversely associated with PCOLCE+ fibroblasts ($\rho = -0.30$, $p = 0.02$) (Fig. 5f). Finally, the proportion of PVMs was associated with PCOLCE+ fibroblasts ($\rho = 0.50$, $p < 0.001$) and inversely associated with myofibroblasts ($\rho = -0.59$, $p < 0.001$) (Fig. 5g). Taken together, we find high correlation between the proportion of T_{EM} cells, macrophages, and fibro-adipogenic cell populations in SAT,

including several cells that are associated with glucose intolerance, suggesting a coordinated shift in multiple cell lineages accompanying changes in metabolic heath.

Transcriptional Polarization of Macrophages and T Cells towards LAM-like and Effector Memory Phenotype

Having demonstrated that glucose intolerance is independently associated with accumulation of IM, LAM, $CD4^+$ T_{EM}, and $CD8^+$ T_{EM}, and inversely associated with PVM, we next examined the transcriptome that defines these cell compartments. We aggregated gene counts for each participant (pseudobulk method) to evaluate the differential gene expression between prediabetic and non-diabetic PWH using a negative binomial generalized linear model implemented in DESeq2[55], adjusting for age, sex and BMI. 644 genes were differentially expressed ($p_{adj} < 0.05$) between macrophages from prediabetic and non-diabetic PWH. Macrophages from prediabetics had higher expression of genes related to lipid processing (*FABP5, MGLL, C3, OXSM, SCD, GSTZ1, DBI, ACOT8, DECR1, ETFB*) and oxidative phosphorylation (*NDUFS5, NDUFAB1, ATP5MC3, UQCR10, COX5B*), and lower expression of genes related to chemotaxis (*CCL8, CXCL1, CCL2, CCL4L2, CCL4, CCL3L1, CXCL8, CCL3,*), TNF inflammatory pathway (*TNF, TNFSF18, TNFRSF1A, TNFRSF21*), and M2-macrophage polarization (*TRIB1, EGR1, EGR2, MRC1, LYVE1, KLF4*) (Fig. 6a, Supplementary Table 8). KEGG gene set enrichment analysis (GSEA) confirmed enrichment of metabolic processing pathways and reduction in pathways related to cytokine-cytokine receptor interaction, chemokine signaling, and IL-17 signaling (Fig. 7b). Individual macrophage subsets had fewer transcriptional differences. PVMs from prediabetic PWH had higher expression of *ID3*, and lower expression of *CCL2* compared with non-diabetic PWH. Several genes related to chemokines and M2-

phenotypic genes (*TRIB1, HMOX1, CCL2, CCL4*) trended towards lower expression in prediabetic PWH ($p_{adj} < 0.1$) (Supplementary Table 8). Pseudotime using Slingshot[56], demonstrated a single trajectory of monocyte-macrophages transitioning into PVMs (Supplementary Fig. 5a and 5b). Using Tradeseq,[57] which fits a negative binomial generalized additive model to each gene, expression of transcription factors associated with M2 phenotype increased along the pseudotime trajectory including *ZNF331, NR4A3, KLF4, KLF2, MAF, MAFB, ATF4, EGR2, CEBPD, JUND,* and *SON* (Fig. 6c). Several of these genes had reduced expression in prediabetic compared with non-diabetic PWH with pseudobulk differential gene expression analysis. Despite their large proportion, IM did not demonstrate any differentially expressed genes, suggesting their accumulation, rather than altered transcriptional regulation, is a major driver of phenotypic differences (Supplementary Table 8). Finally, LAMs in prediabetic PWH had higher expression of inflammatory genes (*MIF, HAMP*) and lipid-processing/metabolic genes (*MTLN, BSCL2, COX6A1, NDUFB3*), and lower expression of several M2 transcription factors (*TRIB1, EGR1, KLF2*) (Supplementary Fig. 5c, Supplementary Table 8). $CD4^+$ T cells in prediabetic PWH had higher expression of markers of activation and effector memory phenotype (*IL32, BATF, CD63, IFITM3, CSTD*) and lower expression of markers related to naïve T cells (*SELL, LEF1, CCR7*) (Fig. 6d). GSEA demonstrated enrichment of pathways related to secretion and cytoskeleton organization (Fig. 6e). $CD8^+$ T cells in prediabetic PWH had higher expression of cytotoxic and activation genes (*GZMA, CD63, CLEC2B*) and a trend towards higher expression of *IFNG* ($p_{adj} = 0.09$) (Fig. 6f).

There were no differentially expressed genes in preadipocytes from prediabetic versus non-diabetic PWH (Supplementary Table 8). Comparison of diabetic with non-diabetic PWH showed similar, but fewer differentially expressed genes between immune cells, which could

reflect treatment effect (Supplementary Table 9). Taken together, macrophages show a transcriptional profile that shifts from an immune regulatory function to a metabolic phenotype in prediabetic PWH. Expression of transcription factors associated with M2 polarization are reduced in prediabetic PWH, suggesting decreased differentiation of monocyte-macrophages into PVMs. The T cell transcriptional profile shifts towards an activated effector memory/antigen presentation phenotype in prediabetic PWH. While most of the differentially expressed genes were unique by cell type, there were overlapping genes between cell types in both higher and lower expressed genes, particularly between $CD4^+$ and $CD8^+$ T cells and between macrophage subsets (Supplementary Fig. 5d, 5e).

Intercellular Gene Programs Related to Interferon-γ, Tumor Necrosis Factor, and Lipid Metabolic Processes Characterize Glucose Intolerance

Based on some overlapping features of gene changes, and an overall shift in transcriptional profile, we next assessed whether there were coordinated, inter-cellular gene expression programs that define the transcriptional patterns associated with glucose intolerance. We employed DIALOGUE, which is a dimensionality reduction technique that identifies gene expression programs between cell types to identify tissue-specific cellular programs[58]. Multicellular program 1 (MP1) was highly associated with normoglycemia while glucose intolerance was inversely related to MP1 (Fig. 7a). Over-representation analysis of the MP1 showed enrichment of genes related to leukocyte differentiation, regulation of T cell activation, and response to oxidative stress in its upregulated compartment. In contrast, MP1 downregulated compartment was enriched in genes related to IFN-γ responses, neutrophil degranulation, and antigen processing and presentation (Fig. 7b). Glucose intolerance was highly related to $CD4^+$ T

cell gene expression pattern (Fig. 7c). In $CD4^+$ T cells, non-diabetic individuals had increased expression of several genes including *CCR7, LDHB, LEF1, SELL, IL21R* and several ribosomal proteins consistent with a less differentiated state, while prediabetic and diabetic individuals had greater expression of genes related to cytotoxicity (*CCL5, CCL4, PRF1*), activation (*IL32, CD40LG, HLA*), and inflammation (*GBP5, IFNG, TNF, IFITM2).* Several individuals classified as non-diabetic or prediabetic were borderline based on dichotomous classification, which could explain why some individuals did not cluster as expected (*e.g.* 1182). Several non-diabetic individuals who clustered with glucose-intolerant individuals (*e.g.* 1159, 1108) were cytomegalovirus (CMV) seropositive and had high proportion of cytotoxic T_{EMRA} cells based on flow cytometry, likely in response to CMV infection. This suggests that while glucose intolerance is highly associated with MP1, other factors can contribute to an inflammatory SAT environment. $CD8^+$ T cells showed a similar expression pattern; however it did not associate as strongly with glucose intolerance (Fig. 7d). The macrophage compartment MP1 expression program was also not as strongly associated with diabetes status as the T cell compartment but did show enrichment of genes associated with M2 polarization (*KLF10, KLF4, MAFF, MAFB, ATF4, EGR1, EGR2*) and chemotaxis (*CCL2, CCL3, CCL4, CCL8*) in MP1 upregulated compartment, and enrichment of genes associated with lipid metabolism (*APOE, TREM2, APOC1*), and IFN-γ (IFNGR2, IFI27, ISG15) in MP1 downregulated compartment (Supplementary Figures 6a-d). Diabetes status was also significantly associated with MP1 in preadipocytes (Supplementary Figure 6e). Genes associated with non-diabetic phenotype included those important for adipogenesis (*CEBPB, GPX3, KLF2, KLF6, HMOX1, EGR1, EGR2, ZFP36*) whereas those associated with glucose intolerance phenotype included genes related to ECM (*TIMP1, POSTN, COL14A1, PLAAT4, PDGFD*). Overall, MP1 differentiates

between normoglycemic individuals with a program enriched for genes related to naïve T cells, immunoregulatory macrophage function, and adipogenesis, as compared to glucose intolerant individuals with a program enriched for genes related to cytotoxicity, inflammation (*TNF*, *IFNG*), cholesterol and lipid metabolism, and ECM deposition.

$CD4^+$ T_{EM} Expressing CD69 are Associated with Changes in Mature Adipocyte Gene Expression

$CD4^+$ T_{EM} proportion and transcriptional expression were strongly associated with glucose intolerance compared with other immune cell types. These cells express CD69, which is often a marker of tissue residency[47]. Given the close association with glucose intolerance and MP1, we next assessed whether these cells are associated with changes in adipocyte gene expression patterns. We performed probe-based RNA transcript quantification of whole adipose tissue biopsies for 77 adipocyte genes using the NanoString platform. We found that both the cytometric sorted $CD4^+CD69^+$ T cells and single-cell $CD4^+$ T_{EM} cell proportions were associated with higher expression of *ADIPOQ, LPL,* and *LEP,* and lower expression of genes related to long-chain fatty acid metabolism (*CPT1B, CYP27A1, SLC27A5, ACAA1*) and GLP1R in whole SAT (Supplementary Table 10). No other immune cell subsets, including macrophage types or $CD8^+$ T_{EM} had a significant relationship with adipocyte gene expression. Taken together, changes in SAT $CD4^+$ tissue resident cell composition are associated with changes in adipocyte gene expression, which suggests a potential mechanistic link between SAT immune cells, mature adipocytes, and development of metabolic phenotypes.

Regulatory Programs Associated with Diabetes in PWH are Also Present in HIV-negative Persons with Diabetes

Finally, we examined whether the regulatory patterns that define glucose intolerance in PWH are similar in diabetic HIV-negative persons. To this end, we recruited 32 diabetic HIV-negative persons with clinical and demographics features similar to the diabetic PWH, and we performed analyses on an integrated dataset of these two groups to assess for differences by HIV status (Supplementary Table 11). We recovered the same cell types in HIV-negative persons observed in the PWH. Compared with the cell distribution of diabetic PWH, HIV-negative persons had fewer lymphoid cells as a proportion of all cell types (Fig. 8a**)**, fewer $CD4^+$ cytotoxic T cells (Fig. 8b), but similar macrophage polarization, fibro-adipogenic cell proportions, and $CD8^+$ T cell distribution. Transcriptionally, T cells and macrophages from diabetic PWH and diabetic HIV-negative persons were similar (Supplementary Table 12). However, the preadipocyte cells were strikingly different with higher expression of gene related to ECM-, genes that impair adipogenesis, and lipid-processing genes in PWH, suggesting impaired adipogenesis and ECM deposition in PWH compared with HIV-negative (Fig. 8c, 8d, Supplementary Table 12). Finally, with the addition of diabetic HIV-negative persons to the intracellular gene correlation, they tended to cluster with glucose intolerant PWH, suggesting a similar pattern of adipose tissue regulation (Fig. 8e). Overall, we find that although HIV induces significant changes to the lymphoid compartment, the pattern of dysregulation in the adipose tissue of diabetics is similar irrespective of HIV status and our findings may be generalizable to the broader population.

Discussion

In this study, we generated a comprehensive single cell molecular atlas of SAT in PWH to uncover compositional and transcriptional patterns that are associated with glucose intolerance. We showed a shift towards LAM and LAM-like macrophages and T_{EM} cells. Transcriptionally, macrophages shifted from an immunoregulatory cytokine profile towards a lipid processing phenotype while $CD4^+$ and $CD8^+$ T cells shifted towards differentiated and effector phenotypes. Intercellular correlation of gene expression demonstrated upregulation of IFN-γ and TNF-related pathways in $CD4^+$ and $CD8^+$ T cells, upregulation of lipid-processing genes in macrophages, and increased expression of fibrotic genes in preadipocytes in PWH with glucose intolerance. $CD4^+$ memory cells expressing CD69 were most strongly associated with glucose intolerance and alterations in adipocyte gene expression, providing a plausible mechanistic link to altered mature adipocyte function and development of metabolic syndrome. Finally, we show that this regulatory pattern is preserved in HIV-negative participants with diabetes. These data suggest our findings may be generalizable and should be further investigated in HIV-negative cohorts.

Our characterization of SAT resident immune cells and fibro-adipogenic precursor cells expand on previous scRNA-seq descriptions of human adipose tissue in HIV-negative persons[14,15,23]. Uniquely, we evaluated the role of glucose intolerance in compositional and transcriptional polarization of adipose tissue and leveraged our large dataset to evaluate the independent contributions of important biological factors including sex, age, and BMI. We showed a coordinated gene expression response that skews towards inflammatory and lipid metabolism phenotype with glucose intolerance, which may perpetuate ongoing adipose tissue inflammation. While we chose scRNA-seq to perform CITE-seq in parallel, current methods for

making single-cell suspensions for scRNA-seq do not capture mature adipocytes. Therefore, we used whole tissue to capture adipocyte gene expression and demonstrate that $CD4^+$ T cells expressing CD69, a marker of tissue residency and a group comprised primarily of T_{EM}, have significant association with the adipocyte transcriptional profile. This could provide a biological basis linking the SAT immune cell changes with overall metabolic health.

Our study had some limitations. The cross-sectional design precluded an assessment of the temporal course of compositional and transcriptional changes, and future longitudinal scRNA-seq studies are needed. Our separation of participants into three groups by glucose intolerance meant some individuals were on the margin between states, though this was addressed, in part, by our analysis of FBG as a continuous endpoint. Additionally, our cohort lacked a non-diabetic or pre-diabetic HIV-negative group. Despite the size of our unbiased molecular atlas of SAT, we may have missed low frequency cells that contribute to inflammation. Finally, it is difficult in clinical studies to account for potential confounders. However, we overcame this with reasonably matched groups and a large overall cohort to model the contributions of important biological factors to composition and transcriptional patterns.

In summary, we found unique SAT compositional and transcriptional changes with glucose intolerance and identified a conserved cellular regulatory program that differentiated non-diabetic and glucose intolerant individuals. Our dataset is publicly available to the research community on an interactive platform (http://vimrg.app.vumc.org/). These data provide insight into the complexity and breadth of SAT cells that may contribute to glucose intolerance and accelerate future investigation into the role of fibro-adipogenic and immune cell interactions that may open new avenues of research and lead to developing therapeutic interventions.

Methods

Study Participants. Participants were members of the HIV, Adipose Tissue Immunology, and Metabolism (HATIM) study developed to evaluate adipose tissue characteristics in the context of HIV infection and metabolic disease (ClinicalTrials.gov registration NCT04451980). PWH were recruited from the Vanderbilt University Medical Center Comprehensive Care Clinic between August 2017 and June 2018, were on antiretroviral therapy (ART) for ≥ 18 months, had virologic suppression (serum HIV-1 RNA quantification < 50 copies/mL) for ≥ 12 months, had a $CD4^+$ T cell count ≥ 350 cells/mm^3 and had no known inflammatory or rheumatologic conditions. Participants were classified as non-diabetic (HbA1c < 5.7% and/or fasting blood glucose [FBG] < 100 mg/dL), pre-diabetic (HbA1c 5.7-6.5% and/or FBG 100-125 mg/dL), or diabetic (HbA1c > 6.4% and/or FBG ≥ 126 mg/dL and/or on anti-diabetic medication) in accordance with the American Diabetes Association criteria [59]. HIV-negative participants with diabetes were simultaneously recruited from the Vanderbilt *ResearchMatch* cohort, and these individuals were group matched by age and BMI with diabetic PWH. All participants underwent a single clinical research visit after a minimum 8-hour fast that included HbA1c and FBG measurement, peripheral blood mononuclear cell (PBMC) collection, fasting plasma collection, and anthropomorphic measurements. All individuals also underwent subcutaneous adipose tissue liposuction as described below. The Vanderbilt Institutional Review Board approved the research, and all participants provided written consent.

Adipose Tissue Collection and Processing. Subcutaneous adipose tissue biopsies were collected approximately 3 centimeters to the right of the umbilicus after anesthetizing the skin with lidocaine/epinephrine and infiltrating 40 mL of sterile saline and lidocaine into the SAT. We collected approximately 5 grams of adipose tissue using a 2.1 mm blunt, side-ported

liposuction catheter (Tulip CellFriendly™ GEMS system Miller Harvester, Tulip Medical Products) designed for extraction of viable adipocytes and stromal vascular fraction (SVF) during cosmetic adipose tissue transfer procedures[60]. Using this method, adipose tissue is recovered in droplets generally < 3 mm in diameter, limiting the need for mechanical dissociation. The tissue was placed in 40-50 mm^3 of cold saline and mixed. Visible blood clots were removed, and the sample was transferred to a 70 µm filter for repeat saline washes with constant stirring. The adipose tissue was then placed in a gentleMACS™ Dissociator (Miltenyi Biotec) followed by incubation with 100 µL of collagenase D (20mg/mL). The SVF was separated using a Ficoll-Paque Plus density gradient. Samples were cryopreserved in fetal bovine serum with 10% DMSO in liquid nitrogen.

Library Preparation and Sequencing. An antibody Total Seq C master mix containing 45 common markers for lineage, memory, and activation was created by adding 0.5 µL of each antibody. Twelve samples, with representative samples from the four metabolic groups (non-diabetic PWH, pre-diabetic and diabetic PWH, and HIV-negative diabetics), were processed at a single time. The samples were quickly thawed and transferred to labeled 15 mL tubes and diluted to 10 ml with phosphate-buffered saline (PBS) before spinning down at 300 G for 10 minutes. The supernatant was aspirated, and the pellet was resuspended in cell staining buffer and transferred to labeled flow tubes. The sample was again spun at 300 G for 10 minutes, and the supernatant was aspirated. Cells were resuspended in 100 µL of staining buffer. Human TruStain FcX Receptor Blocking Solution (5 µL) was added to the tube and incubated at 4 Celsius for 10 minutes. The antibody master mix was spun at 15000 rpm for 5 minutes to remove any aggregates that had formed, and 22.5 µL of the antibody mix was added to each tube of cells and

mixed by flicking the tube. A total of one µL of Total Seq C hashtag antibody was added to the samples, and the samples were incubated at 4 Celsius for 30 minutes. After incubation, the cells were washed three times with Cell Staining Buffer and spun at 300 G for 10 minutes. The cells were resuspended in around 100 µL of PBS with 0.04% bovine serum albumin (BSA). The cells were counted using the Countess II Automated Cell Counter (Thermo Fisher) to determine the suspension volume to transfer to obtain 5,000 cells. Four samples (each with a unique hashtag antibody) were pooled by metabolic status (except non-diabetic and prediabetic samples from PWH which were pooled) together into one tube. The multiplexed single cells were loaded onto a Chromium Single Cell 5' v.2 assay (10x Genomics). Libraries were sequenced on the NovaSeq 6000 S2 platform (Illumina). Illumina bcl files were demultiplexed using bcl2fastq. Raw reads were then aligned to the human genome (hg38) using STAR v. 2.7.2a, and cells were called using Cellranger count (v.6.0.0) with default settings. Souporcell, which leverages single nucleotide variants to assign individual cells to genotypes and generate a VCF file, was used to genetically demultiplex the samples[61]. SoupX was used with default parameters to remove ambient RNA contamination from the count matrice[62].

Quality Control. The R Statistical Programming package Seurat V4 was used to further process the scRNA-seq data[63]. First, cells with > 25% mitochondrial gene expression, < 800 transcript reads, and < 200 genes were filtered out. The threshold of 800 transcript reads per cell was selected because the performance of Souporcell begins to decrease with fewer transcripts[61]. Hashtag oligonucleotides (HTOs) were normalized using centered log-ratio (CLR) transformation, and cells were assigned HTO implemented in the function HTODemux with default parameters[25,64]. We then added the Souporcell assignment to the metadata and linked the

Souporcell cluster designation with the HTO classification, forming a link with the metadata. All cells that were unassigned by Souporcell were removed. To identify heterotypic doublets, we used standard processing of each lane, including normalization and variance stabilization using regularized negative binomial regression (SCTransform), dimensional reduction, and clustering[65]. DoubletFinder[66], was used to identify potential heterotypic doublets in the data using Souporcell designation as the ground truth. Cells that were identified as doublets by Souporcell or DoubletFinder, clusters where > 60% of cells were identified as doublets, and clusters that expressed transcripts from multiple major lineages (endothelial, immune, fibro-adipogenic, vascular), were removed after integrating the datasets.

Cell Clustering and Annotation. Processed individual lanes were merged using the merge function. The gene counts were normalized for each cell by dividing by the total gene counts and multiplying by a factor of 10,000 before applying log-transformation as implemented by the LogNormalize function. Protein expression counts were normalized using the CLR method. Variable genes were identified using the FindVariableFeatures function (nFeatures = 3000), and the data were scaled and centered using the ScaleData function. Principal component analysis (PCA) was performed on the scaled data. The number of principal components (PCs) used for downstream analysis was selected based on elbow plots and heat maps of PC dimensions as implemented in the DimHeatmap function. To reduce the batch effect associated with running multiple 10X lanes, we used the Harmony algorithm on the uncorrected PCs implemented as a Seurat wrapper to integrate across lanes[26]. To evaluate the effectiveness of integration, we used the SCIB pipeline[67]. The overall metric ranking was calculated by the summation of the scaled overall bio-conservation score * 0.6 + batch score * 0.4. We performed clustering on the

Harmony-corrected PCs using FindNeighbors and FindClusters functions. Marker genes for each cluster were determined using the Wilcoxon Rank Sum test implemented in FindAllMarkers.[68] The integrated dataset was then subclustered as described below. After processing each subcluster, they were merged again, and the process described above (except normalization) was repeated to obtain a cell atlas. We performed manual annotation of cell populations based on canonical markers and markers previously identified in scRNA-seq (Supplementary Table 4).

Subclustering Analysis. We subclustered on major cell types, including fibro-adipogenic (*COL1A2, CCDC80*), vascular (*CLDN5, ACTA2*), myeloid (*LYZ, CD68, CD14, CD1C, LILRA4, CLEC9A*), and lymphoid (*CD3, NKG7*). We followed the procedure described previously for each subcluster but did not repeat RNA and protein normalization. Clusters defined by mitochondrial gene expression and/or transcriptional doublets were removed from the analysis. We performed differential gene expression using the FindAllMarkers function implemented in Seurat to identify gene markers for each cell population and included genes that were expressed in 25% or more cells and had a $\log_2$ fold change of 0.25 or greater.

Composition Analysis. Individuals contributing < 30 cells in the subset investigated were excluded. We compared cell composition between disease states for each subcluster by evaluating each cell type as a proportion of total cells in the subcluster. We assessed whether cell type changes were significant between non-diabetic PWH and prediabetic PWH, and between non-diabetic PWH and diabetic PWH using the Wilcoxon Rank Sums test. P values were adjusted for multiple comparisons using Benjamini-Hochberg procedure.

To evaluate the independent relationship of cell proportions with BMI, age, and measures of glucose intolerance (HbA1c, FBG), we used partial spearman's correlation implemented in PResiduals[69]. We visualized the results by plotting spearman's ρ per cluster superimposed on the uniform manifold approximation and projection (UMAP). We used the same method to evaluate the inter-cellular proportion relationships. To evaluate the independent relationship of female sex with cell proportions, we used an ordinal linear regression with cell proportion as the outcome and sex (male reference) as the independent variable adjusted for age, BMI, and diabetes status. The β coefficient was converted to an odds ratio (female: male) going from the 25th to 75th percentile (proportion) and visualized by plotting on the UMAP as above.

Transcriptional Analysis. To evaluate differentially expressed genes between non-diabetic and pre-diabetic PWH, we aggregated gene counts (psuedobulk) for each individual using scuttle[70]. We then used a negative binomial generalized linear model implemented in DESeq2 to evaluate differentially expressed genes adjusting for age, sex, and BMI. We used clusterProfiler to perform gene set enrichment analysis using the Kyoto Encyclopedia of Genes and Genomes (KEGG) and Gene Ontology (GO) biological processes to identify pathways that were enriched in prediabetic compared with non-diabetic PWH.[71]

Pseudotime Analysis. The R package Slingshot,[56] was used to assess the pseudo-time trajectory of PVM. Monocyte-macrophages were specified as the root cluster with the dimensionality reduction produced by UMAP. To identify temporally dynamic genes, we fit a generalized additive model (GAM) using a negative binomial additive model implemented in the R package tradeSeq[57]. We used the associationTest function with l2fc set to 2 to identify genes significantly

changing along the pseudo-time, defined as FDR-adjusted p-value < 0.05. The genes were then ordered according to pseudo-time and plotted by scaled expression using ComplexHeatmap[72].

Multicellular Gene Expression Programs. To evaluate for a coordinate cellular program that characterizes glucose intolerance, we used DIALOGUE[58], evaluating the cell types we previously identified as associated with glucose intolerance including $CD4^+$ and $CD8^+$ T cells, macrophage subsets, preadipocytes, and fibroblast cells. DIALOGUE was run with default settings. The multi-level models were fit by glucose intolerance status, and adjusted for technical variability, sex, age, and BMI. Average scaled expression of top genes from MP1 were sorted by expression and samples were plotted with hierarchical clustering (rows) and labeled with clinical variables including BMI, age, sex, and measures of glucose intolerance using ComplexHeatmap.

Whole Adipose Tissue Messenger RNA Expression. The detailed methods for these samples have been published elsewhere[73]. Briefly, messenger RNA (mRNA) was extracted from cryopreserved SAT with Qiagen RNeasy Lipid Tissue Kit after mechanical lysis. The NanoString nCounter Plex platform (NanoString, Seattle, WA) was used to quantify mRNA transcripts for 77 genes related to adipocyte function. The mRNA count was normalized using eight synthetic spike-ins for negative control and six synthetic spike-ins for positive controls. The coefficient of variation (CV) was calculated for control genes. First, the mean of the negative controls was used as the background level and subtracted from each gene count. The normalization factor for the mRNA content was calculated using the geometric mean of a set of pre-specific housekeeping genes. The count data were then divided by the normalization factor to generate counts normalized to the geometric mean of housekeeping genes. The normalized gene

count data was then log2-transformed, and a linear regression model was used to assess the relationship between the cell-type proportion with mRNA expression. The cell proportion was the independent variable, and the log2-transformed mRNA count was the dependent variable, adjusted for age, sex, BMI, metabolic status, and batch. Benjamini-Hochberg was used to correct for multiple comparisons.

Data Availability. Raw sequencing files, cell metadata, and fully integrated Seurat objects are available via the NCBI GEO with the primary accession code GSE198809. The data is available on an interactive ShinyCell-based[74], web application at https://vimrg.app.vumc.org/.

Code Availability. All code processing and analyses code for this paper are available on github at https://github.com/VIMRG/AdiposeTissueAtlas.

Acknowledgement

This work was supported by National Institutes of Health grants R01DK112262 (JRK and CNW), R01HL145372 (JAK), K23HL156759 (CNW, JRK), the Vanderbilt Clinical and Translational Science Award from NCRR/NIH grant UL1RR024975, the Vanderbilt Infection Pathogenesis and Epidemiology Research Training Program (VIPER) grant T32AI007474, the Vanderbilt Scholars in HIV and Heart, Lung, Blood and Sleep Research (V-SCHoLARS) grant K12HL143956, the Vanderbilt Institute for Clinical and Translational Research supported by grant KL2TR002245 from the National Center for Advancing Translational Sciences, the Tennessee Center for AIDS Research grant P30AI110527 (SAM, CNW, JRK, SAK), the Doris Duke Charitable Foundation grant 2021193 (CNW, JRK) and the Burroughs Welcome Fund grant 1021480 (CNW, JRK). The funding authorities had no role in study design, data collection, analysis, interpretation, the decision to publish, or manuscript preparation. We also thank the participants of the HATIM study. The figures were created with BioRender.com.

Author Contributions

Conceptualization, C.N.W., J.R.K., S.A.M.; Methodology, C.N.W., J.R.K., S.A.M., R.D.G., J.D.S., A.C., R.R., C.W., J.A.K., S.S.B.; Formal Analysis, S.S.B., C.N.W., J.R.K., S.A.K., J.A.K., R.R., F.Y., R.F.; Investigation, C.N.W., C.W., J.D.S., R.D.G., L.H.; Writing – Original Draft, S.S.B., C.N.W., J.R.K., J.A.K.; Writing – Review & Editing, S.S.B., C.N.W., J.A.K., J.R.K., S.A.M., S.A.K., C.L.G., M.M., L.H., J.D.S., C.W., R.F., F.Y.; Funding Acquisition, C.N.W., J.R.K., S.A.M.

Declaration of Interests

J.A.K. consults for Boehringer Ingelheim, Janssen, and Bristol-Myers-Squibb, serves on the scientific advisory board for APIE Therapeutics, and provides non-financial study support to Genentech. J.R.K. has served as a consultant to Gilead Sciences, Merck, ViiV Healthcare, Theratechnologies, and Janssen, and has received research support from Gilead Sciences and Merck. C.N.W. serves on the scientific advisory board for ViiV Healthcare.

Main Figure Legends

Figure 1. Single-cell RNA sequencing reveals complex cellular structure of subcutaneous white adipose tissue. a, Schematic overview of study design. Twenty HIV+ non-diabetic, 19 HIV+ prediabetic, and 20 HIV+ diabetic participants underwent abdominal subcutaneous adipose tissue harvesting with liposuction. Tissue was processed with collagenase and dissociated. Single-cell suspensions from each participant were hashed and labeled with CITE-seq antibodies before multiplexing in groups of four. 10x libraries were generated using the Chromium platform and sequenced on Illumina NovaSeq 6000. The bioinformatic pipeline included demultiplexing, quality control, dimensional reduction and clustering, and transcriptional analysis. **b**, Uniform Manifold Approximation and Projection (UMAP) of 177,942 cells from 59 individuals after removal of doublets and quality control, with manual annotation of cell clusters based on canonical gene markers. **c**, UMAP after harmony integration grouped by disease status showing successful integration; HIV+ non-diabetic (green), HIV+ prediabetic (blue), and HIV+ diabetic (yellow). **d**, Gene expression projected onto the UMAP identifying major cell types including fibro-adipogenic (*COL1A2, CCDC80*), vascular (*CLDN5, ACTA2*), myeloid (CD68, CD1C), and T cell and natural killer cells (*CD3E, NKG7*). **e**, Boxplot showing the proportion of major cell categories (fibro-adipogenic, vascular, lymphoid, and myeloid) as a percentage of total cells split by disease status (n = 59) (HIV+ non-diabetic, green; HIV+ prediabetic, blue; HIV+ diabetic, yellow). The horizontal black line represents the median, the box shows the lower and upper quartile limits and the whiskers are 1.5x the interquartile range.

Abbreviations: cMo, classical monocyte; cDC1, conventional dendritic cell type 1; cDC2B, conventional dendritic cell type 2B; DC, dendritic cell; EC, endothelial cell; ECM, extracellular

matrix; EndoMT, endothelial-mesenchymal transitional; ILC, innate lymphoid cell; IM, intermediate macrophage; ISG+, interferon; LAM, lipid-associated macrophage; Mac, macrophage; mNK, mature natural killer; Mo, monocyte; NK, natural killer; nMo, non-classical monocyte; pDC, plasmacytoid dendritic cell; PVM, perivascular macrophage; VSMC, vascular smooth muscle cells

Figure 2. Analysis of Subsets Shows Delineation of Cell Types That are Important for Adipose Tissue Function. a, Uniform Manifold Approximation and Projection (UMAP) of myeloid cells (n = 40,585 cells) from 59 individuals after subsetting and reclustering showing 14 distinct cell types/states. **b**, Dot plot showing selected myeloid gene markers on the x-axis and cell type on the y-axis. The dot size reflects the percentage of cells expressing the gene while the color reflects the scaled average expression. **c,** UMAP of T cells, natural killer cells, and innate lymphoid cells (n = 28,061 cells) from 59 individuals after subsetting and reclustering showing 16 distinct cell types/states. **d**, Dot plot showing selected Lymphoid gene markers on the x-axis and cell type on the y-axis. The dot size reflects the percentage of cells expressing the gene while the color reflects the scaled average expression. **e**, UMAP of fibro-adipogenic cells (n = 51,029 cells) from 59 individuals after subsetting and reclustering. **f**, Dot plot showing selected fibro-adipogenic gene markers on the x-axis and cell type on the y-axis. The dot size reflects the percentage of cells expressing the gene while the color reflects the scaled average expression. **g**, UMAP of vascular cells (n = 55,534 cells) from 59 individuals after subsetting and reclustering. **h**, Dot plot showing selected vascular gene markers on the x-axis and cell type on the y-axis. The dot size reflects the percentage of cells expressing the gene while the color reflects the scaled average expression.

Abbreviations: cMo, classical monocyte; cDC1, conventional dendritic cell type 1; cDC2B, conventional dendritic cell type 2B; DC, dendritic cell; EC, endothelial cell; ECM, extracellular matrix; EndoMT, endothelial-mesenchymal transitional; ILC, innate lymphoid cell; IM, intermediate macrophage; IM, intermediate macrophage; ISG+, interferon; LAM, lipid-associated macrophage; Mac, macrophage; mNK, mature natural killer; Mo, monocyte; NK, natural killer; nMo, non-classical monocyte; pDC, plasmacytoid dendritic cell; PVM, perivascular macrophage; VSMC, vascular smooth muscle

Figure 3. Lipid-associated, intermediate macrophages, and $CD4^+$ and $CD8^+$ T effector memory proportions are associated with glucose intolerance. a, Boxplot showing the proportion of macrophage types split by disease state (HIV+ non-diabetic, green; HIV+ prediabetic, blue; HIV+ diabetic, yellow) (n = 54). The horizontal black line represents the median, the box shows the lower and upper quartile limits and the whiskers are 1.5x the interquartile range. **b,** Partial spearman's correlations between fasting blood glucose (FBG) or hemoglobin A1c (HbA1c) and macrophage cell proportions. Spearman's r for the biological factor (FBG or HbA1c) and each cluster proportion was calculated. The r value (blue, negative; red, positive) for each cluster was plotted onto the macrophage uniform manifold approximation and projection (UMAP). Clusters with significant correlation ($p < 0.05$) are labeled. **c**, Partial spearman's correlation between FBG or HbA1c and cluster proportion plotted onto the myeloid UMAP. **d,** Boxplot showing the proportion of $CD8^+$ T cell subsets as a proportion of total $CD8^+$ T cells (n = 47). **e,** Partial spearman's correlation between FBG or HbA1c and cluster proportion plotted onto the $CD8^+$ T cell UMAP. **f**, Boxplot showing the proportion of $CD4^+$ T cell subsets as

a proportion of total $CD4^+$ T cells (n = 44). **g**, Partial spearman's correlation between FBG or HbA1c and cluster proportion plotted onto the $CD4^+$ T cell UMAP.

Abbreviations: IM, intermediate macrophage; LAM, lipid-associated macrophage; Mo-Mac, monocyte-macrophage; PVM, perivascular macrophage; TCM, T central memory; TEM, T effector memory

Figure 4. Body Mass Index and Sex Are Associated with Compositional Changes in Immune and Fibro-adipogenic Cells. a-d, Partial spearman's correlations. Spearman's r for the biological factor (body mass index [BMI] or age) and each cluster proportion was calculated. The r value (blue, negative; red, positive) for each cluster was plotted onto the uniform manifold approximation and projection (UMAP). Clusters with significant correlation ($p < 0.05$) are labeled. BMI and age plotted onto **a,** Myeloid UMAP, **b,** $CD4^+$ T cell UMAP, **c**, $CD8^+$ T cell UMAP, and **d,** Fibro-adipogenic UMAP. **e-h,** Ordinal linear regression with cluster proportion as the outcome and sex as the independent variable adjusted for age, BMI, and diabetes status. The regression coefficient for sex was converted into an odds ratio (female:male) and plotted per cluster onto the UMAP. Odds ratio female: male plotted onto **e**, Macrophage UMAP, **f**, $CD4^+$ T cell UMAP, **g,** $CD8^+$ T cell UMAP, and **h,** fibro-adipogenic UMAP. Abbreviations: PC, progenitor cell; BMI, body mass index; FIB, fibroblast; IM, intermediate macrophage; Mac, macrophage; Mo, monocyte; LAM, lipid-associated macrophage; pDC, plasmacytoid dendritic cell; PreAd, preadipocyte; PVM, perivascular macrophage; TCM, T central memory

Figure 5. Inter-Cellular Correlation of Proportions with Cells Associated with Glucose Intolerance. a-g, Partial spearman's correlations. Spearman's r for the immune cell proportion

of interest and each cluster proportion was calculated. The r value (blue, negative; red, positive) for each cluster was plotted onto the uniform manifold approximation and projection (UMAP). Clusters with significant correlation ($p < 0.05$) are labeled. **a,** Spearman's r for $CD4^+$ T effector memory (T_{EM}) proportion and myeloid clusters plotted onto the myeloid uniform manifold approximation and projection (UMAP). **b,** Spearman's r for $CD8^+$ T_{EM} cell proportion and myeloid clusters plotted onto the myeloid UMAP. **c**, Spearman's r for $CD4^+$ T_{EM} proportion and fibro-adipogenic clusters plotted onto the fibro-adipogenic UMAP. **d,** Spearman's r for $CD8^+$ T_{EM} proportion and fibro-adipogenic clusters plotted onto the fibro-adipogenic UMAP. **e**, Spearman's r for intermediate macrophage proportion and fibro-adipogenic clusters plotted onto the fibro-adipogenic UMAP. **f**, Spearman's r for lipid-associated macrophage proportion and fibro-adipogenic clusters plotted onto the fibro-adipogenic UMAP. **g,** Spearman's r for perivascular macrophage proportion and fibro-adipogenic clusters plotted onto the fibro-adipogenic UMAP. Abbreviations: BMI, body mass index; cDC1, conventional dendritic cell type 1; cMo, classical monocyte; ECM, extracellular matrix; FIB, fibroblast; IM, intermediate macrophage; Mac, macrophage; Mo, monocyte; MyoFIB, myofibroblast; LAM, lipid-associated macrophage; PC, progenitor cell; pDC, plasmacytoid dendritic cell; PreAd, preadipocyte; PVM, perivascular macrophage.

Figure 6. Transcriptional Shift from Immunoregulatory to Metabolic Phenotype in Macrophages and Effector Memory Phenotype in T cells with Glucose Intolerance. a, Macrophage volcano plot with average Log_2 fold change (x-axis) and $-log_{10}$ p-value (y-axis) for prediabetic vs non-diabetic (reference) PWH. Genes that had ≥ 0.25 log_2 fold change and adjusted p-value < 0.05 were colored red (higher expression) and blue (lower expression). **b,**

Gene set enrichment analysis (GSEA) using the KEGG database. The top 5 and bottom 5 enriched pathways were included with normalized enrichment score (NES) on x-axis and descriptive term on y-axis. Dot size represents the number of gene hits in the pathway and dot color represents the $-\log_{10}$ p-value. **C,** Ordered and smoothed transcription factor gene expression (scaled) along the pseudotime trajectory for monocyte-macrophage to perivascular macrophage. Selected genes were significantly differentially expression along the pseudotime with $\geq \log_2(2)$ fold change according to TradSeq. **d**, $CD4^+$ T cell volcano plot with average Log_2 fold change (x-axis) and $-\log_{10}$ p-value (y-axis) for prediabetic vs non-diabetic (reference) PWH. Genes that had ≥ 0.25 $\log_2$ fold change and adjusted p-value < 0.05 were colored red (higher expression) and blue (lower expression). **e,** Gene ontology GSEA for the top 7 and bottom *7* enriched pathways with normalized enrichment score (NES) on x-axis and descriptive term on y-axis. Dot size represents the number of gene hits in the pathway and dot color represents the $-\log_{10}$ p-value. **f**, $CD8^+$ T cell volcano plot with average Log_2 fold change (x-axis) and $-\log_{10}$ p-value (y-axis) for prediabetic vs non-diabetic (reference) PWH. Genes that had ≥ 0.25 $\log_2$ fold change and adjusted p-value < 0.05 were colored red (higher expression) and blue (lower expression). Abbreviations: NES, normalized enrichment score.

Figure 7. Inter-Cellular Gene Correlation Reveals an Interferon-g , tumor necrosis factor, and lipid metabolism Expression Pattern with Glucose Intolerance. a, Distribution of expression scores for each cell type component for multicellular program (MP) 1 with kernel density estimates. **b,** Over-representation analysis using Gene Ontology for genes in MP1 with higher expression (Up) and lower expression (Down). Dot size represents the number of gene hits in the pathway and dot color represents the $-\log_{10}$ p-value. **c,** Average scaled expression of

top $CD4^+$ T cell genes from MP1 sorted by expression (columns), across samples plotted with hierarchical clustering (rows) and labeled with clinical variables including body mass index (BMI), age, sex, and measures of glucose intolerance. **d**, Average scaled expression of top $CD8^+$ T cell genes from MP1 sorted by expression (columns), across samples plotted with hierarchical clustering (rows) and labeled with clinical variables including BMI, age, sex, and measures of glucose intolerance. Abbreviations: FIB, fibroblast; IM, intermediate macrophage; Mac, macrophage; Mo, monocyte; LAM, lipid-associated macrophage; PreAd, preadipocyte; PVM, perivascular macrophage.

Figure 8. HIV-negative diabetic and HIV-positive diabetic Have Similar Macrophage and T Effector Memory Cell Polarization and Preserved Inter-cellular Gene Expression Program. a, Boxplot showing the proportion of major cell categories (stromal, vascular, lymphoid, and myeloid) as a percentage of total cells split by disease status (n = 51). **b,** Boxplot showing the proportion of macrophage subsets as a percentage of total macrophage cells split by disease status (n = 51). **c**, Preadipocyte volcano plot with average Log_2 fold change (x-axis) and $-log_{10}$ p-value (y-axis) for HIV-positive diabetic vs HIV- diabetic (reference) persons. Genes that had ≥ 0.25 log_2 fold change and adjusted p-value < 0.05 were colored red (higher expression) and blue (lower expression). **d,** Gene set enrichment analysis (GSEA) using the Gene Ontology database. The top 6 and bottom 6 enriched pathways were included with normalized enrichment score (NES) on x-axis and descriptive term on y-axis. Dot size represents the number of gene hits in the pathway and dot color represents the $-log_{10}$ p-value. **e,** Average scaled expression of top $CD4^+$ T cell genes from MP1 sorted by expression (columns), across samples plotted with hierarchical clustering (rows) and labeled with clinical variables including

body mass index (BMI), age, sex, and measures of glucose intolerance. Abbreviations: BMI, body mass index; FBG, fasting blood glucose; HbA1c, hemoglobin A1c; IM, intermediate macrophage; Mac, macrophage; Mo, monocyte; LAM, lipid-associated macrophage; PVM, perivascular macrophage

Supplementary Figures

Supplementary Figure 1. Bioinformatic Pipeline and Quality Metrics. a, Flow diagram of bioinformatic pipeline. Cells were called using the Cell Ranger count function with default settings. Soupx was used to remove ambient RNA and the corrected count matrices were used to create a Seurat object. Simultaneously, Souporcell was used to genetically demultiplex the samples. Doublets identified by Souporcell were used as ground truths for DoubletFinder. Next, each Seurat object underwent quality control filtering and downstream dimensional reduction and clustering. The processed objects were then integrated using Harmony correction on the principal components prior to clustering. Cells identified as doublets, clusters with > 60% doublets, or expression of 2 or more major lineages were removed. Cells were subclustered based on major cell lineages and transcriptional doublets were iteratively removed prior to reintegration. **b,** Barplot graph showing each lane (x-axis) and number of cells (y-axis). The graph is split by the total barcodes identified by Cell Ranger (red) and the cells remaining after doublet and QC removal (green). **c,** Distribution of read counts per cell (y-axis) by lane (x-axis). **d,** Distribution of the number of features (genes) per cell (y-axis) by lane (x-axis). **e,** Overall integration metric ranking generated by the SCIB pipeline. Unintegrated, harmony integration with feature selection (HVG) and no feature selection, as well as scaled and unscaled were input in the SCIB pipeline. The overall rank was computed by overall batch score (0.5) and

bioconservation (0.6) that were scaled for comparison. **f,** Dot plot with selected genes on the x axis and cell type on the y axis. The size of the dot represents the percentage of cells with expression of that gene and the color of the dot represents the average expression level for that gene.

Supplementary Figure 2. CITE-seq and Pathway Analysis Support Cell Annotation. a, Antibody derived tags (ADT) for CD11C, CD1C, CD16, and CD71 plotted as the average cluster expression onto the uniform manifold approximation and projection (UMAP) for myeloid cells. **b**, UMAP of IM, PVM, Mo-Mac, and LAMs from 59 individuals. **c,** Gene Ontology (GO) over-representation analysis with macrophage subtype on the x-axis and GO pathway on the y-axis. The size of the circle denotes the number of genes assigned to the pathway while the color denotes the p-value. **d**, ADT for CD16, CD27, CD4, CD45RA, CD57, and CD8, plotted as the per cluster average expression superimposed on the lymphoid UMAP. **e**, UMAP of $CD4^+$ T cells (n = 8,435 cells) subset from all T cells. **f**, ADT for CD27, CD45RA, CD57, and CD69, plotted as the per cluster average expression superimposed on the $CD4^+$ T cell UMAP. **g**, UMAP of $CD8^+$ T cells (n = 11,356 cells) subset from all T cells. **h**, ADT for CD27, CD45RA, CD57, and CD69, plotted as the per cluster average expression superimposed on the $CD8^+$ T cell UMAP. Abbreviations: cMo, classical monocyte; cDC1, conventional dendritic cell type 1; cDC2B, conventional dendritic cell type 2B; DC, dendritic cell; ECM, extracellular matrix; ILC, innate lymphoid cell; IM, intermediate macrophage; IM, intermediate macrophage; LAM, lipid-associated macrophage; Mac, macrophage; mNK, mature natural killer; Mo, monocyte; NK, natural killer; nMo, non-classical monocyte; pDC, plasmacytoid dendritic cell; PVM, perivascular macrophage

Supplementary Figure 3. Cell Type Proportions by Diabetes Status. a, Partial spearman's correlations between fasting blood glucose (FBG) or hemoglobin A1c (HbA1c) and lymphoid cell proportions. Spearman's r for the biological factor (FBG or HbA1c) and each cluster proportion was calculated. The r value (blue, negative; red, positive) for each cluster was plotted onto the macrophage uniform manifold approximation and projection (UMAP). Clusters with significant correlation ($p < 0.05$) are labeled. **b,** Partial spearman's correlation between FBG or HbA1c and cluster proportion plotted onto the fibro-adipogenic UMAP. **c**, Boxplot showing the proportion of fibroblast types split by disease state (HIV+ non-diabetic, green; HIV+ prediabetic, blue; HIV+ diabetic, yellow) ($n = 59$). The horizontal black line represents the median, the box shows the lower and upper quartile limits and the whiskers are 1.5x the interquartile range. **d,** Partial spearman's correlation between FBG or HbA1c and cluster proportion plotted onto the vascular UMAP. Abbreviations: ECM, extracellular matrix; FIB, fibroblast; mNK, mature natural killer.

Supplementary Figure 4. Relationship of Body Mass Index, Age, and Sex to Other Cell Populations. a-b, Partial spearman's correlations. Spearman's r for the biological factor (body mass index [BMI] or age) and each cluster proportion was calculated. The r value (blue, negative; red, positive) for each cluster was plotted onto the uniform manifold approximation and projection (UMAP). Clusters with significant correlation ($p < 0.05$) are labeled. BMI and age plotted onto **a,** Lymphoid UMAP, **b,** Vascular UMAP. **c-e,** Ordinal linear regression with cluster proportion as the outcome and sex as the independent variable adjusted for age, BMI, and diabetes status. The regression coefficient for sex was converted into an odds ratio (female:

male) and plotted per cluster onto the UMAP. Odds ratio female: male plotted onto **c**, Myeloid UMAP, **d**, Lymphoid UMAP, **f,** Vascular UMAP. Abbreviations: BMI, body mass index; DC, dendritic cell; EndoMT, Endothelial-Mesenchymal Transition; IM Cap, Intermediate Capillary Endothelial;.mNK, mature natural killer.

Supplementary Figure 5. Transcriptional Profile of Adipose Tissue Immune Cells a, Slingshot trajectory with monocyte-macrophage as the root embedded on the UMAP and, **b**, Slingshot pseudotime. **c,** Gene set enrichment analysis (GSEA) using the Gene Ontology database. The top 6 and bottom 6 enriched pathways were included with normalized enrichment score (NES) on x-axis and descriptive term on y-axis. Dot size represents the number of gene hits in the pathway and dot color represents the $-\log_{10}$ p-value. **d,** Upset plot for genes with higher expression in prediabetic compared with non-diabetic PWH across cell types. The x-axis shows the set size for each cell type (total number of differentially expressed genes in the cell type) and the y-axis shows the intersection size with other cells (number of shared genes). **e**, Upset plot for genes with lower expression in prediabetic compared with non-diabetic PWH across cell types. The x-axis shows the set size for each cell type (total number of differentially expressed genes in the cell type) and the y-axis shows the intersection size with other cells (number of shared genes). Abbreviations: NES, normalized enrichment score.

Supplementary Figure 6. Multicellular Program Using DIALOGUE Identifies Expression Patterns Associated with Glucose Intolerance. a-f, Average scaled expression of top genes from MP1 sorted by expression (columns), across samples plotted with hierarchical clustering (rows) and labeled with clinical variables including body mass index (BMI), age, sex, and

measures of glucose intolerance. **a,** Perivascular macrophages. **b,** Lipid-associated macrophages. **c,** Intermediate macrophages. **d**, Monocyte-macrophages. **e,** Preadipocytes. Abbreviations: BMI, body mass index; FBG, fasting blood glucose; HbA1c, hemoglobin A1c.

References

1 Jaacks, L. M. *et al.* The obesity transition: stages of the global epidemic. *Lancet Diabetes Endocrinol* **7**, 231-240, doi:10.1016/S2213-8587(19)30026-9 (2019).

2 Saeedi, P. *et al.* Global and regional diabetes prevalence estimates for 2019 and projections for 2030 and 2045: Results from the International Diabetes Federation Diabetes Atlas, 9(th) edition. *Diabetes Res Clin Pract* **157**, 107843, doi:10.1016/j.diabres.2019.107843 (2019).

3 Nansseu, J. R., Bigna, J. J., Kaze, A. D. & Noubiap, J. J. Incidence and Risk Factors for Prediabetes and Diabetes Mellitus Among HIV-infected Adults on Antiretroviral Therapy: A Systematic Review and Meta-analysis. *Epidemiology* **29**, 431-441, doi:10.1097/EDE.0000000000000815 (2018).

4 Shah, A. S. V. *et al.* Global Burden of Atherosclerotic Cardiovascular Disease in People Living With HIV: Systematic Review and Meta-Analysis. *Circulation* **138**, 1100-1112, doi:10.1161/CIRCULATIONAHA.117.033369 (2018).

5 Putcharoen, O. *et al.* New-onset diabetes in HIV-treated adults: predictors, long-term renal and cardiovascular outcomes. *AIDS* **31**, 1535-1543, doi:10.1097/QAD.0000000000001496 (2017).

6 Herrin, M. *et al.* Weight Gain and Incident Diabetes Among HIV-Infected Veterans Initiating Antiretroviral Therapy Compared With Uninfected Individuals. *J Acquir Immune Defic Syndr* **73**, 228-236, doi:10.1097/QAI.0000000000001071 (2016).

7 Sax, P. E. *et al.* Weight Gain Following Initiation of Antiretroviral Therapy: Risk Factors in Randomized Comparative Clinical Trials. *Clin Infect Dis* **71**, 1379-1389, doi:10.1093/cid/ciz999 (2020).

8 Otake, K. *et al.* HIV-1 Nef protein in the nucleus influences adipogenesis as well as viral transcription through the peroxisome proliferator-activated receptors. *AIDS* **18**, 189-198, doi:10.1097/00002030-200401230-00007 (2004).

9 Butt, A. A. *et al.* HIV infection and the risk of diabetes mellitus. *AIDS* **23**, 1227-1234, doi:10.1097/QAD.0b013e32832bd7af (2009).

10 Ghaben, A. L. & Scherer, P. E. Adipogenesis and metabolic health. *Nat Rev Mol Cell Biol* **20**, 242-258, doi:10.1038/s41580-018-0093-z (2019).

11 Lumeng, C. N., Bodzin, J. L. & Saltiel, A. R. Obesity induces a phenotypic switch in adipose tissue macrophage polarization. *J Clin Invest* **117**, 175-184, doi:10.1172/JCI29881 (2007).

12 Nishimura, S. *et al.* CD8+ effector T cells contribute to macrophage recruitment and adipose tissue inflammation in obesity. *Nat Med* **15**, 914-920, doi:10.1038/nm.1964 (2009).

13 Feuerer, M. *et al.* Lean, but not obese, fat is enriched for a unique population of regulatory T cells that affect metabolic parameters. *Nat Med* **15**, 930-939, doi:10.1038/nm.2002 (2009).

14 Emont, M. P. *et al.* A single-cell atlas of human and mouse white adipose tissue. *Nature*, doi:10.1038/s41586-022-04518-2 (2022).

15 Hildreth, A. D. *et al.* Single-cell sequencing of human white adipose tissue identifies new cell states in health and obesity. *Nat Immunol* **22**, 639-653, doi:10.1038/s41590-021-00922-4 (2021).

16 Neuhaus, J. *et al.* Markers of inflammation, coagulation, and renal function are elevated in adults with HIV infection. *J Infect Dis* **201**, 1788-1795, doi:10.1086/652749 (2010).

17 Damouche, A. *et al.* Adipose Tissue Is a Neglected Viral Reservoir and an Inflammatory Site during Chronic HIV and SIV Infection. *PLoS Pathog* **11**, e1005153, doi:10.1371/journal.ppat.1005153 (2015).

18 Couturier, J. *et al.* Human adipose tissue as a reservoir for memory CD4+ T cells and HIV. *AIDS* **29**, 667-674, doi:10.1097/QAD.0000000000000599 (2015).

19 Wanjalla, C. N. *et al.* Adipose Tissue in Persons With HIV Is Enriched for CD4(+) T Effector Memory and T Effector Memory RA(+) Cells, Which Show Higher CD69 Expression and CD57, CX3CR1, GPR56 Co-expression With Increasing Glucose Intolerance. *Front Immunol* **10**, 408, doi:10.3389/fimmu.2019.00408 (2019).

20 Wanjalla, C. N. *et al.* Single-cell analysis shows that adipose tissue of persons with both HIV and diabetes is enriched for clonal, cytotoxic, and CMV-specific CD4+ T cells. *Cell Rep Med* **2**, 100205, doi:10.1016/j.xcrm.2021.100205 (2021).

21 Appay, V. & Sauce, D. Immune activation and inflammation in HIV-1 infection: causes and consequences. *J Pathol* **214**, 231-241, doi:10.1002/path.2276 (2008).

22 Hazenberg, M. D., Hamann, D., Schuitemaker, H. & Miedema, F. T cell depletion in HIV-1 infection: how CD4+ T cells go out of stock. *Nat Immunol* **1**, 285-289, doi:10.1038/79724 (2000).

23 Vijay, J. *et al.* Single-cell analysis of human adipose tissue identifies depot and disease specific cell types. *Nat Metab* **2**, 97-109, doi:10.1038/s42255-019-0152-6 (2020).

24 Sarvari, A. K. *et al.* Plasticity of Epididymal Adipose Tissue in Response to Diet-Induced Obesity at Single-Nucleus Resolution. *Cell Metab* **33**, 437-453 e435, doi:10.1016/j.cmet.2020.12.004 (2021).

25 Stoeckius, M. *et al.* Simultaneous epitope and transcriptome measurement in single cells. *Nat Methods* **14**, 865-868, doi:10.1038/nmeth.4380 (2017).

26 Korsunsky, I. *et al.* Fast, sensitive and accurate integration of single-cell data with Harmony. *Nat Methods* **16**, 1289-1296, doi:10.1038/s41592-019-0619-0 (2019).

27 Travaglini, K. J. *et al.* A molecular cell atlas of the human lung from single-cell RNA sequencing. *Nature* **587**, 619-625, doi:10.1038/s41586-020-2922-4 (2020).

28 Jaitin, D. A. *et al.* Lipid-Associated Macrophages Control Metabolic Homeostasis in a Trem2-Dependent Manner. *Cell* **178**, 686-698 e614, doi:10.1016/j.cell.2019.05.054 (2019).

29 Hao, Y. *et al.* Integrated analysis of multimodal single-cell data. *Cell* **184**, 3573-3587 e3529, doi:10.1016/j.cell.2021.04.048 (2021).

30 Merrick, D. *et al.* Identification of a mesenchymal progenitor cell hierarchy in adipose tissue. *Science* **364**, doi:10.1126/science.aav2501 (2019).

31 Hill, D. A. *et al.* Distinct macrophage populations direct inflammatory versus physiological changes in adipose tissue. *Proc Natl Acad Sci U S A* **115**, E5096-E5105, doi:10.1073/pnas.1802611115 (2018).

32 Lee, B. C. *et al.* Adipose Natural Killer Cells Regulate Adipose Tissue Macrophages to Promote Insulin Resistance in Obesity. *Cell Metab* **23**, 685-698, doi:10.1016/j.cmet.2016.03.002 (2016).

33 Goldberg, E. L. *et al.* Ketogenesis activates metabolically protective gammadelta T cells in visceral adipose tissue. *Nat Metab* **2**, 50-61, doi:10.1038/s42255-019-0160-6 (2020).

34 Brestoff, J. R. *et al.* Group 2 innate lymphoid cells promote beiging of white adipose tissue and limit obesity. *Nature* **519**, 242-246, doi:10.1038/nature14115 (2015).

35 Piera-Velazquez, S. & Jimenez, S. A. Endothelial to Mesenchymal Transition: Role in Physiology and in the Pathogenesis of Human Diseases. *Physiol Rev* **99**, 1281-1324, doi:10.1152/physrev.00021.2018 (2019).

36 Amano, S. U. *et al.* Local proliferation of macrophages contributes to obesity-associated adipose tissue inflammation. *Cell Metab* **19**, 162-171, doi:10.1016/j.cmet.2013.11.017 (2014).

37 Cinti, S. *et al.* Adipocyte death defines macrophage localization and function in adipose tissue of obese mice and humans. *J Lipid Res* **46**, 2347-2355, doi:10.1194/jlr.M500294-JLR200 (2005).

38 Macdougall, C. E. *et al.* Visceral Adipose Tissue Immune Homeostasis Is Regulated by the Crosstalk between Adipocytes and Dendritic Cell Subsets. *Cell Metab* **27**, 588-601 e584, doi:10.1016/j.cmet.2018.02.007 (2018).

39 Russo, L. & Lumeng, C. N. Properties and functions of adipose tissue macrophages in obesity. *Immunology* **155**, 407-417, doi:10.1111/imm.13002 (2018).

40 Jan, V. *et al.* Altered fat differentiation and adipocytokine expression are inter-related and linked to morphological changes and insulin resistance in HIV-1-infected lipodystrophic patients. *Antivir Ther* **9**, 555-564 (2004).

41 Shikuma, C. M. *et al.* The role of HIV and monocytes/macrophages in adipose tissue biology. *J Acquir Immune Defic Syndr* **65**, 151-159, doi:10.1097/01.qai.0000435599.27727.6c (2014).

42 Cipolletta, D. *et al.* PPAR-gamma is a major driver of the accumulation and phenotype of adipose tissue Treg cells. *Nature* **486**, 549-553, doi:10.1038/nature11132 (2012).

43 Deiuliis, J. *et al.* Visceral adipose inflammation in obesity is associated with critical alterations in tregulatory cell numbers. *PLoS One* **6**, e16376, doi:10.1371/journal.pone.0016376 (2011).

44 Fabbrini, E. *et al.* Association between specific adipose tissue CD4+ T-cell populations and insulin resistance in obese individuals. *Gastroenterology* **145**, 366-374 e361-363, doi:10.1053/j.gastro.2013.04.010 (2013).

45 Winer, S. *et al.* Normalization of obesity-associated insulin resistance through immunotherapy. *Nat Med* **15**, 921-929, doi:10.1038/nm.2001 (2009).

46 Bofill, M. *et al.* Increased numbers of primed activated CD8+CD38+CD45RO+ T cells predict the decline of CD4+ T cells in HIV-1-infected patients. *AIDS* **10**, 827-834, doi:10.1097/00002030-199607000-00005 (1996).

47 Sathaliyawala, T. *et al.* Distribution and compartmentalization of human circulating and tissue-resident memory T cell subsets. *Immunity* **38**, 187-197, doi:10.1016/j.immuni.2012.09.020 (2013).

48 Schwalie, P. C. *et al.* A stromal cell population that inhibits adipogenesis in mammalian fat depots. *Nature* **559**, 103-108, doi:10.1038/s41586-018-0226-8 (2018).

49 Sun, W. *et al.* snRNA-seq reveals a subpopulation of adipocytes that regulates thermogenesis. *Nature* **587**, 98-102, doi:10.1038/s41586-020-2856-x (2020).

50 Burl, R. B. *et al.* Deconstructing Adipogenesis Induced by beta3-Adrenergic Receptor Activation with Single-Cell Expression Profiling. *Cell Metab* **28**, 300-309 e304, doi:10.1016/j.cmet.2018.05.025 (2018).

51 Oguri, Y. *et al.* CD81 Controls Beige Fat Progenitor Cell Growth and Energy Balance via FAK Signaling. *Cell* **182**, 563-577 e520, doi:10.1016/j.cell.2020.06.021 (2020).

52 Brestoff, J. R. *et al.* Intercellular Mitochondria Transfer to Macrophages Regulates White Adipose Tissue Homeostasis and Is Impaired in Obesity. *Cell Metab* **33**, 270-282 e278, doi:10.1016/j.cmet.2020.11.008 (2021).

53 Tabib, T. *et al.* Myofibroblast transcriptome indicates SFRP2(hi) fibroblast progenitors in systemic sclerosis skin. *Nat Commun* **12**, 4384, doi:10.1038/s41467-021-24607-6 (2021).

54 Sun, K., Tordjman, J., Clement, K. & Scherer, P. E. Fibrosis and adipose tissue dysfunction. *Cell Metab* **18**, 470-477, doi:10.1016/j.cmet.2013.06.016 (2013).

55 Love, M. I., Huber, W. & Anders, S. Moderated estimation of fold change and dispersion for RNA-seq data with DESeq2. *Genome Biol* **15**, 550, doi:10.1186/s13059-014-0550-8 (2014).

56 Street, K. *et al.* Slingshot: cell lineage and pseudotime inference for single-cell transcriptomics. *BMC Genomics* **19**, 477, doi:10.1186/s12864-018-4772-0 (2018).

57 Van den Berge, K. *et al.* Trajectory-based differential expression analysis for single-cell sequencing data. *Nat Commun* **11**, 1201, doi:10.1038/s41467-020-14766-3 (2020).

58 Jerby-Arnon, L. & Regev, A. DIALOGUE maps multicellular programs in tissue from single-cell or spatial transcriptomics data. *Nat Biotechnol*, doi:10.1038/s41587-022-01288-0 (2022).

59 American Diabetes, A. 2. Classification and Diagnosis of Diabetes: Standards of Medical Care in Diabetes-2020. *Diabetes Care* **43**, S14-S31, doi:10.2337/dc20-S002 (2020).

60 Alexander, R. W. & Harrell, D. B. Autologous fat grafting: use of closed syringe microcannula system for enhanced autologous structural grafting. *Clin Cosmet Investig Dermatol* **6**, 91-102, doi:10.2147/CCID.S40575 (2013).

61 Heaton, H. *et al.* Souporcell: robust clustering of single-cell RNA-seq data by genotype without reference genotypes. *Nat Methods* **17**, 615-620, doi:10.1038/s41592-020-0820-1 (2020).

62 Young, M. D. & Behjati, S. SoupX removes ambient RNA contamination from droplet-based single-cell RNA sequencing data. *Gigascience* **9**, doi:10.1093/gigascience/giaa151 (2020).

63 Stuart, T. *et al.* Comprehensive Integration of Single-Cell Data. *Cell* **177**, 1888-1902 e1821, doi:10.1016/j.cell.2019.05.031 (2019).

64 Stoeckius, M. *et al.* Cell Hashing with barcoded antibodies enables multiplexing and doublet detection for single cell genomics. *Genome Biol* **19**, 224, doi:10.1186/s13059-018-1603-1 (2018).

65 Hafemeister, C. & Satija, R. Normalization and variance stabilization of single-cell RNA-seq data using regularized negative binomial regression. *Genome Biol* **20**, 296, doi:10.1186/s13059-019-1874-1 (2019).

66 McGinnis, C. S., Murrow, L. M. & Gartner, Z. J. DoubletFinder: Doublet Detection in Single-Cell RNA Sequencing Data Using Artificial Nearest Neighbors. *Cell Syst* **8**, 329-337 e324, doi:10.1016/j.cels.2019.03.003 (2019).

67 Luecken, M. D. *et al.* Benchmarking atlas-level data integration in single-cell genomics. *Nat Methods* **19**, 41-50, doi:10.1038/s41592-021-01336-8 (2022).

68 Finak, G. *et al.* MAST: a flexible statistical framework for assessing transcriptional changes and characterizing heterogeneity in single-cell RNA sequencing data. *Genome Biol* **16**, 278, doi:10.1186/s13059-015-0844-5 (2015).

69 Lui, Q., Shepherd, B. & Li, C. PResiduals: An R package for residual analysis using probability-scale residuals. *Jounral of Statistical Software* **94**, 1-27 (2020).

70 McCarthy, D. J., Campbell, K. R., Lun, A. T. & Wills, Q. F. Scater: pre-processing, quality control, normalization and visualization of single-cell RNA-seq data in R. *Bioinformatics* **33**, 1179-1186, doi:10.1093/bioinformatics/btw777 (2017).

71 Wu, T. *et al*. clusterProfiler 4.0: A universal enrichment tool for interpreting omics data. *Innovation (Camb)* **2**, 100141, doi:10.1016/j.xinn.2021.100141 (2021).

72 Gu, Z., Eils, R. & Schlesner, M. Complex heatmaps reveal patterns and correlations in multidimensional genomic data. *Bioinformatics* **32**, 2847-2849, doi:10.1093/bioinformatics/btw313 (2016).

73 Gabriel, C. L. *et al.* Hepatic Steatosis and Ectopic Fat Are Associated With Differences in Subcutaneous Adipose Tissue Gene Expression in People With HIV. *Hepatol Commun* **5**, 1224-1237, doi:10.1002/hep4.1695 (2021).

74 Ouyang, J. F., Kamaraj, U. S., Cao, E. Y. & Rackham, O. J. L. ShinyCell: Simple and sharable visualisation of single-cell gene expression data. *Bioinformatics*, doi:10.1093/bioinformatics/btab209 (2021).

Table 1. Cohort Characteristics.

	HIV+ non-diabetic (n = 20)	**HIV+ prediabetic (n = 19)**	**HIV+ diabetic (n = 20)**	**P value**
Age, years	46 (40, 52)	42 (38, 54)	55 (48, 62)	0.053
Race, black (%)	7 (35)	8 (42)	23 (39)	0.99
Sex, female	7 (35)	4 (21)	5 (25)	0.60
Body mass index (kg/m^2)	31.0 (28.6, 34.7)	29.4 (28.4, 34.2)	33.2 (30.2, 37.8)	0.079
Fasting blood glucose (mg/dl)	88 (82, 92)	111 (102, 122)	184 (120, 242)	< 0.001
Hemoglobin A1c (%)	5.3 (5.1, 5.4)	5.5 (5.1, 5.9)	7.8 (6.4, 9.5)	< 0.001
Metformin use (%)	0 (0)	0 (0)	12 (60)	< 0.001
CD4 count at enrollment	784 (660, 941)	684 (544, 1000)	893 (724, 1102)	0.53
Thymidine analogue exposure (%)	5 (26)	2 (11)	4 (22)	0.45
Integrase-based regimen (%)	13 (65)	11 (58)	11 (55)	0.80

Continuous variables are shown as median value with interquartile range. Categorical variables are shown as number and percent.

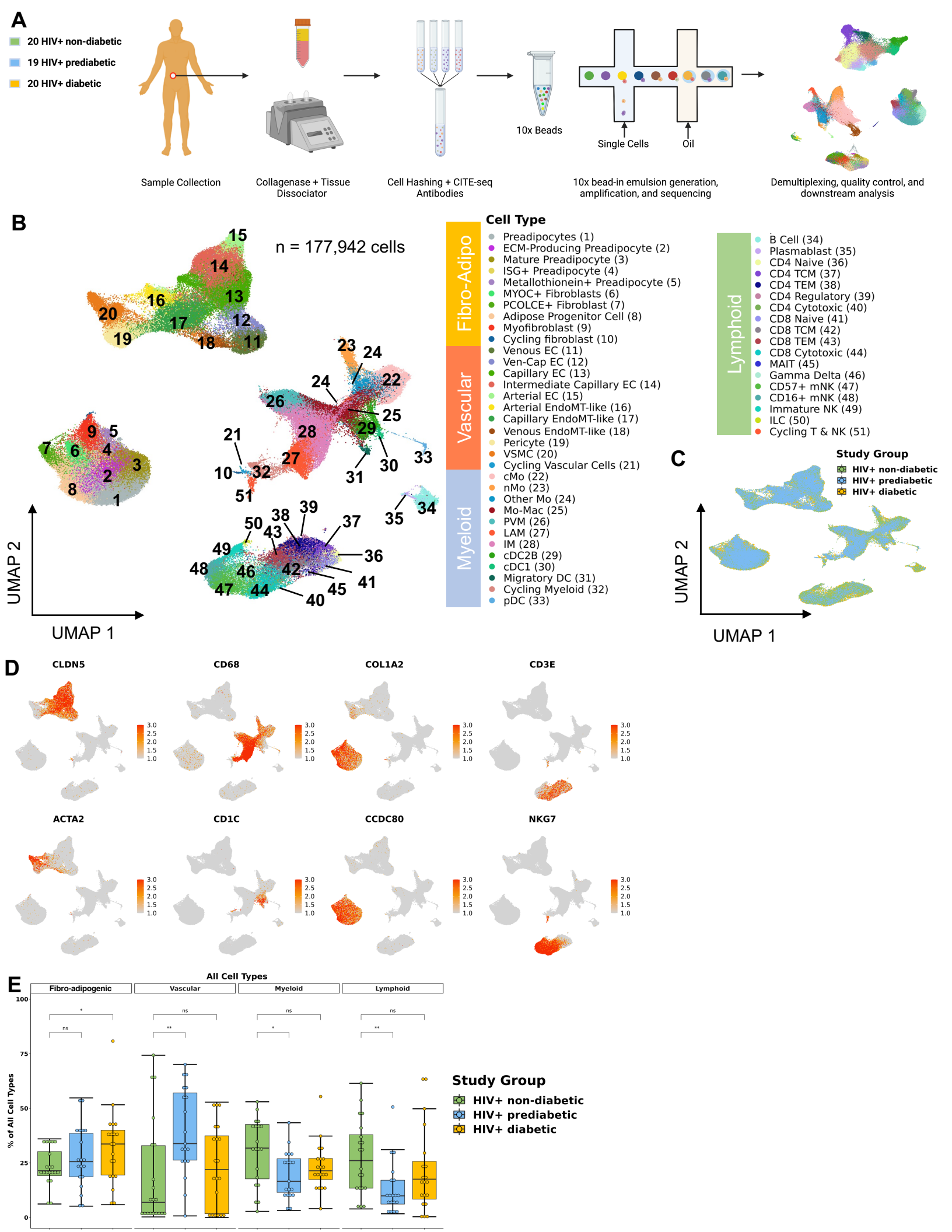
A
20 HIV+ non-diabetic
19 HIV+ prediabetic
20 HIV+ diabetic
10x Beads
Single Cells
Oil
Sample Collection
Collagenase + Tissue Dissociator
Cell Hashing + CITE-seq Antibodies
10x bead-in emulsion generation, amplification, and sequencing
Demultiplexing, quality control, and downstream analysis
B
n = 177,942 cells
UMAP 2
UMAP 1
Cell Type
Fibro-Adipo
Vascular
Myeloid
Lymphoid
Preadipocytes (1)
ECM-Producing Preadipocyte (2)
Mature Preadipocyte (3)
ISG+ Preadipocyte (4)
Metallothionein+ Preadipocyte (5)
MYOC+ Fibroblasts (6)
PCOLCE+ Fibroblast (7)
Adipose Progenitor Cell (8)
Myofibroblast (9)
Cycling fibroblast (10)
Venous EC (11)
Ven-Cap EC (12)
Capillary EC (13)
Intermediate Capillary EC (14)
Arterial EC (15)
Arterial EndoMT-like (16)
Capillary EndoMT-like (17)
Venous EndoMT-like (18)
Pericyte (19)
VSMC (20)
Cycling Vascular Cells (21)
cMo (22)
nMo (23)
Other Mo (24)
Mo-Mac (25)
PVM (26)
LAM (27)
IM (28)
cDC2B (29)
cDC1 (30)
Migratory DC (31)
Cycling Myeloid (32)
pDC (33)
B Cell (34)
Plasmablast (35)
CD4 Naive (36)
CD4 TCM (37)
CD4 TEM (38)
CD4 Regulatory (39)
CD4 Cytotoxic (40)
CD8 Naive (41)
CD8 TCM (42)
CD8 TEM (43)
CD8 Cytotoxic (44)
MAIT (45)
Gamma Delta (46)
CD57+ mNK (47)
CD16+ mNK (48)
Immature NK (49)
ILC (50)
Cycling T & NK (51)
C
Study Group
HIV+ non-diabetic
HIV+ prediabetic
HIV+ diabetic
UMAP 2
UMAP 1
D
CLDN5
CD68
COL1A2
CD3E
ACTA2
CD1C
CCDC80
NKG7
3.0
2.5
2.0
1.5
1.0
E
All Cell Types
Fibro-adipogenic
Vascular
Myeloid
Lymphoid
% of All Cell Types
100
75
50
25
0
ns
*
**
Study Group
HIV+ non-diabetic
HIV+ prediabetic
HIV+ diabetic

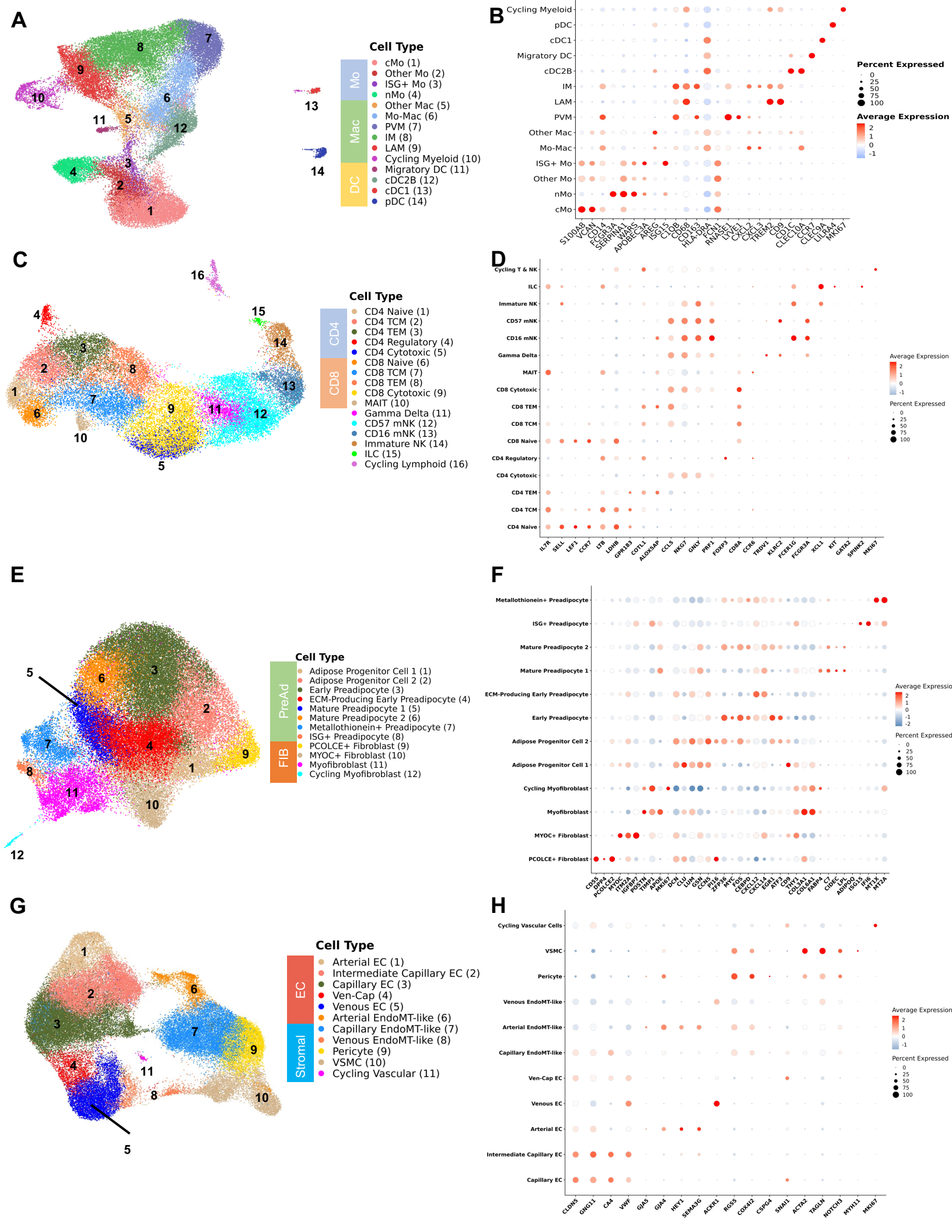
A
Cell Type
Mo
Mac
DC
cMo (1)
Other Mo (2)
ISG+ Mo (3)
nMo (4)
Other Mac (5)
Mo-Mac (6)
PVM (7)
IM (8)
LAM (9)
Cycling Myeloid (10)
Migratory DC (11)
cDC2B (12)
cDC1 (13)
pDC (14)
B
Cycling Myeloid
pDC
cDC1
Migratory DC
cDC2B
IM
LAM
PVM
Other Mac
Mo-Mac
ISG+ Mo
Other Mo
nMo
cMo
S100A8 VCAN CD14 FCGR3A SERPINA1 WARS APOBEC3A AREG ISG15 C1QB CD68 CD163 HLA-DRA FCN1 RNASE1 LYVE1 CXCL2 CXCL3 TREM2 CD9 CD1C CLEC10A CCR7 CLEC9A LILRA4 MKI67
Percent Expressed
0
25
50
75
100
Average Expression
2
1
0
-1
C
Cell Type
CD4
CD8
CD4 Naive (1)
CD4 TCM (2)
CD4 TEM (3)
CD4 Regulatory (4)
CD4 Cytotoxic (5)
CD8 Naive (6)
CD8 TCM (7)
CD8 TEM (8)
CD8 Cytotoxic (9)
MAIT (10)
Gamma Delta (11)
CD57 mNK (12)
CD16 mNK (13)
Immature NK (14)
ILC (15)
Cycling Lymphoid (16)
D
Cycling T & NK
ILC
Immature NK
CD57 mNK
CD16 mNK
Gamma Delta
MAIT
CD8 Cytotoxic
CD8 TEM
CD8 TCM
CD8 Naive
CD4 Regulatory
CD4 Cytotoxic
CD4 TEM
CD4 TCM
CD4 Naive
IL7R SELL LEF1 CCR7 LTB LDHB GPR183 COTL1 ALOX5AP CCL5 NKG7 GNLY PRF1 FOXP3 CD8A CCR6 TRDV1 KLRC2 FCER1G FCGR3A XCL1 KIT GATA2 SPINK2 MKI67
Average Expression
2
1
0
-1
Percent Expressed
0
25
50
75
100
E
Cell Type
PreAd
FIB
Adipose Progenitor Cell 1 (1)
Adipose Progenitor Cell 2 (2)
Early Preadipocyte (3)
ECM-Producing Early Preadipocyte (4)
Mature Preadipocyte 1 (5)
Mature Preadipocyte 2 (6)
Metallothionein+ Preadipocyte (7)
ISG+ Preadipocyte (8)
PCOLCE+ Fibroblast (9)
MYOC+ Fibroblast (10)
Myofibroblast (11)
Cycling Myofibroblast (12)
F
Metallothionein+ Preadipocyte
ISG+ Preadipocyte
Mature Preadipocyte 2
Mature Preadipocyte 1
ECM-Producing Early Preadipocyte
Early Preadipocyte
Adipose Progenitor Cell 2
Adipose Progenitor Cell 1
Cycling Myofibroblast
Myofibroblast
MYOC+ Fibroblast
PCOLCE+ Fibroblast
CD55 DPP4 PCOLCE2 MYOC ITM2A IGFBP7 POSTN TIMP1 APOE MKI67 DCN CLU LUM GSN CCN5 PI16 ZFP36 MYC FOS CEBPD CXCL12 CXCL14 EGR1 ATF3 CD9 THY1 COL3A1 COL6A1 FABP4 C7 CIDEC LPL ADIPOQ ISG15 IFI6 MT1X MT2A
Average Expressio
2
1
0
-1
-2
Percent Expressed
0
25
50
75
100
G
Cell Type
EC
Stromal
Arterial EC (1)
Intermediate Capillary EC (2)
Capillary EC (3)
Ven-Cap (4)
Venous EC (5)
Arterial EndoMT-like (6)
Capillary EndoMT-like (7)
Venous EndoMT-like (8)
Pericyte (9)
VSMC (10)
Cycling Vascular (11)
H
Cycling Vascular Cells
VSMC
Pericyte
Venous EndoMT-like
Arterial EndoMT-like
Capillary EndoMT-like
Ven-Cap EC
Venous EC
Arterial EC
Intermediate Capillary EC
Capillary EC
CLDN5 GNG11 CA4 VWF GJA5 GJA4 HEY1 SEMA3G ACKR1 RGS5 COX4I2 CSPG4 SNAI1 ACTA2 TAGLN NOTCH3 MYH11 MKI67
Average Expression
2
1
0
-1
Percent Expressed
0
25
50
75
100

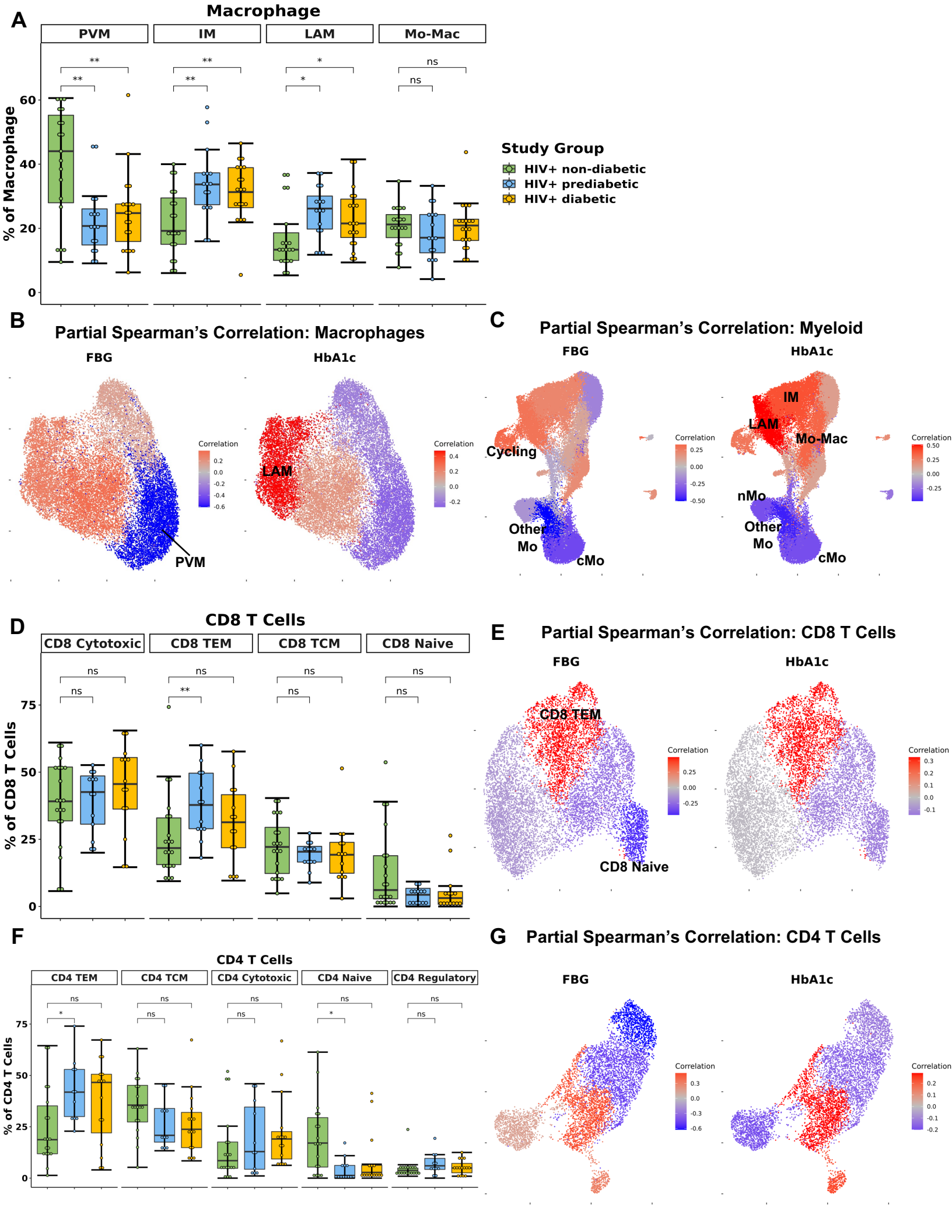
A
Macrophage
PVM
IM
LAM
Mo-Mac
% of Macrophage
Study Group
HIV+ non-diabetic
HIV+ prediabetic
HIV+ diabetic
B
Partial Spearman's Correlation: Macrophages
FBG
HbA1c
Correlation
LAM
PVM
C
Partial Spearman's Correlation: Myeloid
FBG
HbA1c
Cycling
Other Mo
cMo
IM
LAM
Mo-Mac
nMo
Other Mo
cMo
D
CD8 T Cells
CD8 Cytotoxic
CD8 TEM
CD8 TCM
CD8 Naive
% of CD8 T Cells
E
Partial Spearman's Correlation: CD8 T Cells
FBG
HbA1c
CD8 TEM
CD8 Naive
F
CD4 T Cells
CD4 TEM
CD4 TCM
CD4 Cytotoxic
CD4 Naive
CD4 Regulatory
% of CD4 T Cells
G
Partial Spearman's Correlation: CD4 T Cells
FBG
HbA1c

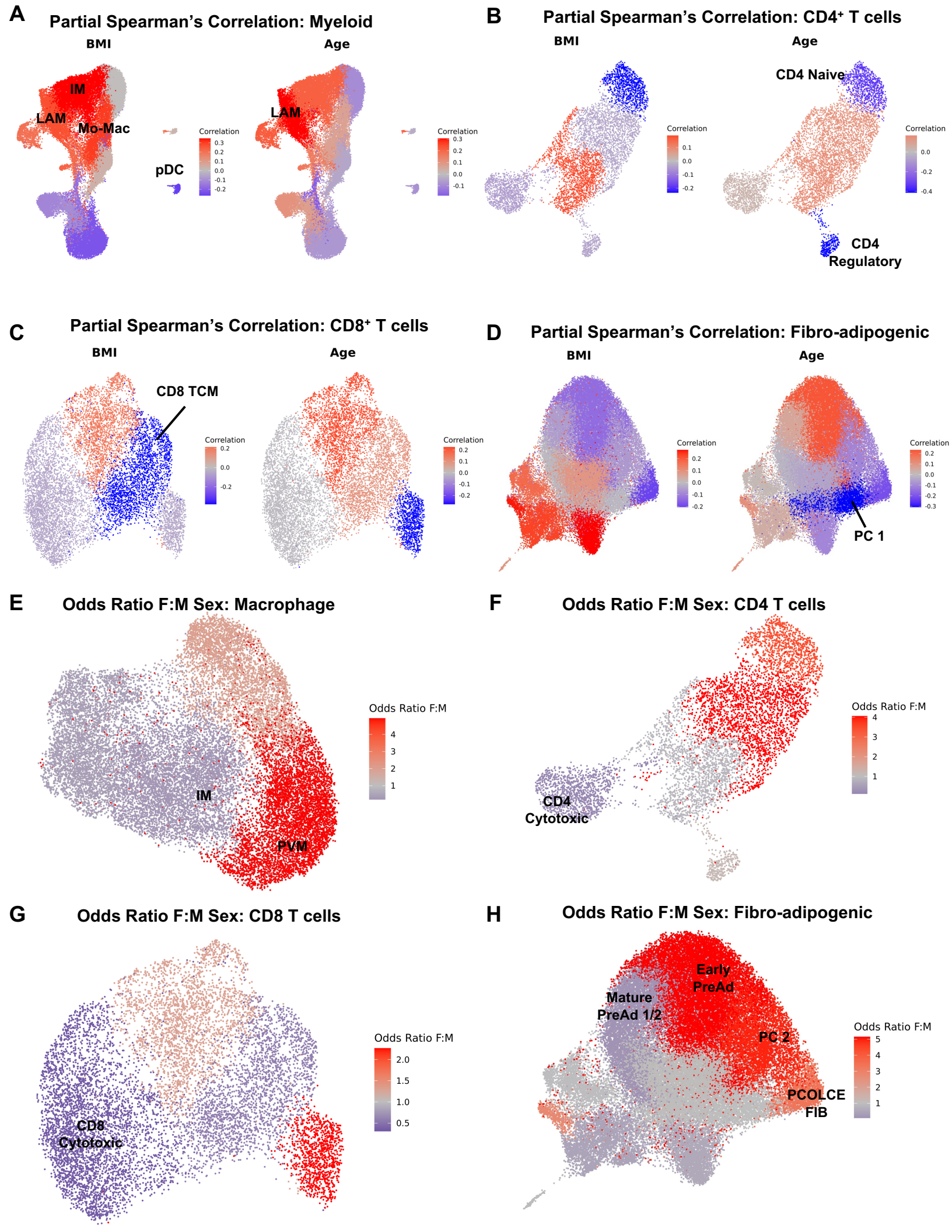
A
Partial Spearman's Correlation: Myeloid
BMI
Age
IM
LAM
Mo-Mac
pDC
LAM
Correlation
0.3
0.2
0.1
0.0
-0.1
-0.2
B
Partial Spearman's Correlation: CD4+ T cells
BMI
Age
CD4 Naive
CD4
Regulatory
Correlation
0.1
0.0
-0.1
-0.2
0.0
-0.2
-0.4
C
Partial Spearman's Correlation: CD8+ T cells
BMI
Age
CD8 TCM
Correlation
0.2
0.0
-0.2
0.2
0.1
0.0
-0.1
-0.2
D
Partial Spearman's Correlation: Fibro-adipogenic
BMI
Age
PC 1
Correlation
0.2
0.1
0.0
-0.1
-0.2
0.2
0.1
0.0
-0.1
-0.2
-0.3
E
Odds Ratio F:M Sex: Macrophage
IM
PVM
Odds Ratio F:M
4
3
2
1
F
Odds Ratio F:M Sex: CD4 T cells
CD4
Cytotoxic
Odds Ratio F:M
4
3
2
1
G
Odds Ratio F:M Sex: CD8 T cells
CD8
Cytotoxic
Odds Ratio F:M
2.0
1.5
1.0
0.5
H
Odds Ratio F:M Sex: Fibro-adipogenic
Early
PreAd
Mature
PreAd 1/2
PC 2
PCOLCE
FIB
Odds Ratio F:M
5
4
3
2
1

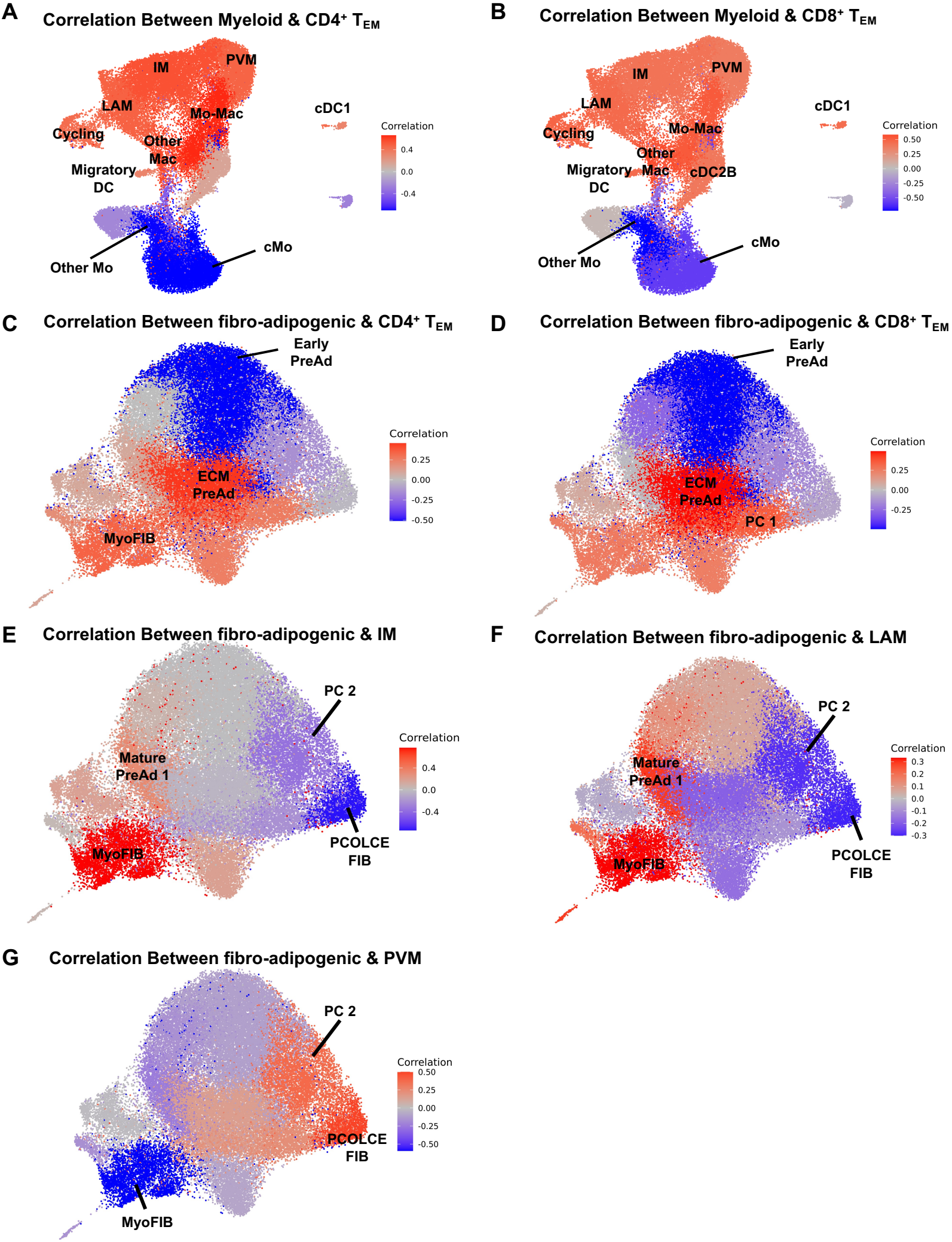
A
Correlation Between Myeloid & CD4+ TEM
IM
PVM
LAM
Mo-Mac
Cycling
Other Mac
Migratory DC
cDC1
Other Mo
cMo
Correlation
0.4
0.0
-0.4
B
Correlation Between Myeloid & CD8+ TEM
IM
PVM
LAM
Cycling
Mo-Mac
Other Mac
Migratory DC
cDC2B
cDC1
Other Mo
cMo
Correlation
0.50
0.25
0.00
-0.25
-0.50
C
Correlation Between fibro-adipogenic & CD4+ TEM
Early PreAd
ECM PreAd
MyoFIB
Correlation
0.25
0.00
-0.25
-0.50
D
Correlation Between fibro-adipogenic & CD8+ TEM
Early PreAd
ECM PreAd
PC 1
Correlation
0.25
0.00
-0.25
E
Correlation Between fibro-adipogenic & IM
PC 2
Mature PreAd 1
MyoFIB
PCOLCE FIB
Correlation
0.4
0.0
-0.4
F
Correlation Between fibro-adipogenic & LAM
PC 2
Mature PreAd 1
MyoFIB
PCOLCE FIB
Correlation
0.3
0.2
0.1
0.0
-0.1
-0.2
-0.3
G
Correlation Between fibro-adipogenic & PVM
PC 2
PCOLCE FIB
MyoFIB
Correlation
0.50
0.25
0.00
-0.25
-0.50

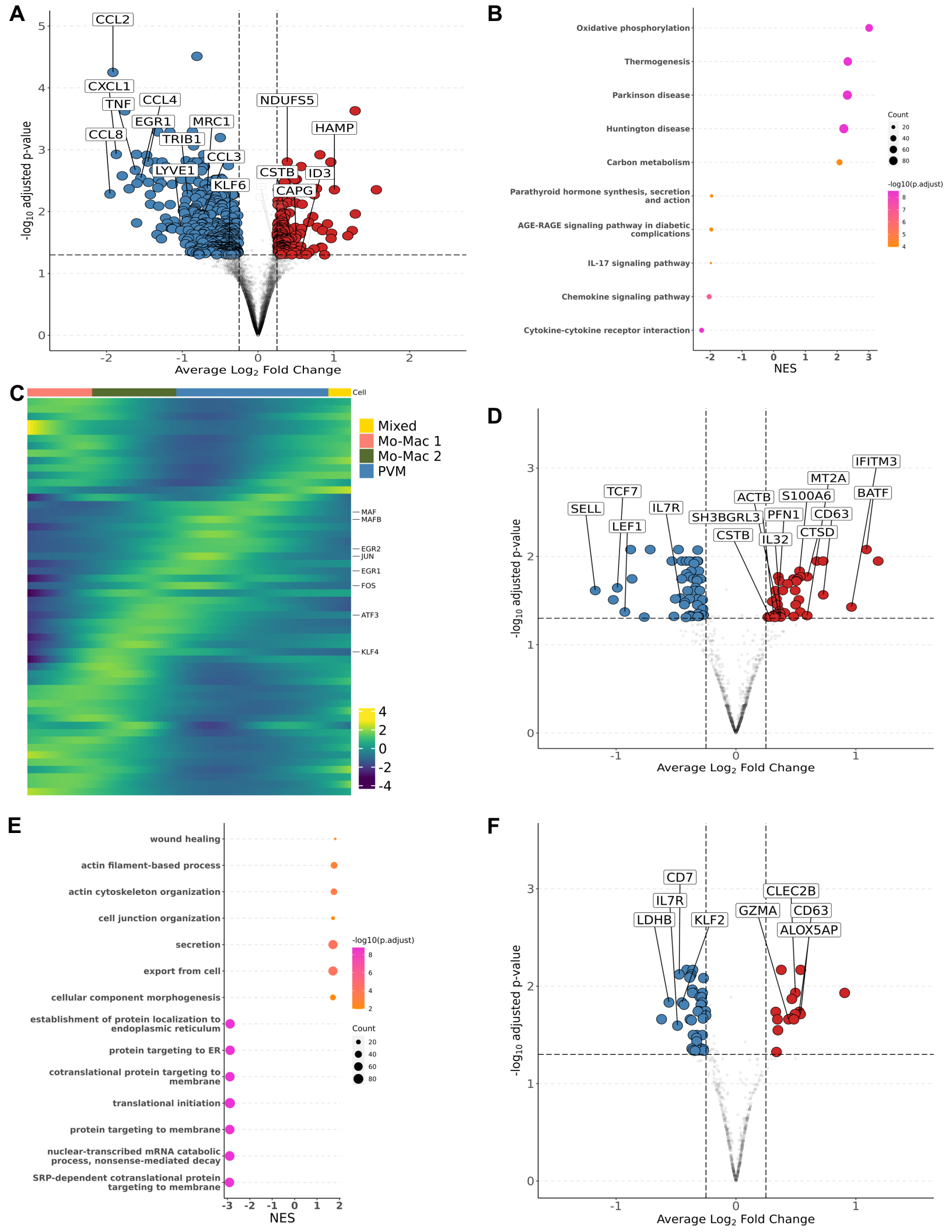
A
CCL2
CXCL1
TNF
CCL4
EGR1
MRC1
CCL8
TRIB1
CCL3
LYVE1
KLF6
NDUFS5
HAMP
CSTB
ID3
CAPG
-log10 adjusted p-value
Average Log2 Fold Change
B
Oxidative phosphorylation
Thermogenesis
Parkinson disease
Huntington disease
Carbon metabolism
Parathyroid hormone synthesis, secretion and action
AGE-RAGE signaling pathway in diabetic complications
IL-17 signaling pathway
Chemokine signaling pathway
Cytokine-cytokine receptor interaction
Count
-log10(p.adjust)
NES
C
Cell
Mixed
Mo-Mac 1
Mo-Mac 2
PVM
MAF
MAFB
EGR2
JUN
EGR1
FOS
ATF3
KLF4
D
IFITM3
MT2A
BATF
TCF7
SELL
IL7R
ACTB
S100A6
SH3BGRL3
PFN1
CD63
LEF1
CSTB
IL32
CTSD
-log10 adjusted p-value
Average Log2 Fold Change
E
wound healing
actin filament-based process
actin cytoskeleton organization
cell junction organization
secretion
export from cell
cellular component morphogenesis
establishment of protein localization to endoplasmic reticulum
protein targeting to ER
cotranslational protein targeting to membrane
translational initiation
protein targeting to membrane
nuclear-transcribed mRNA catabolic process, nonsense-mediated decay
SRP-dependent cotranslational protein targeting to membrane
-log10(p.adjust)
Count
NES
F
CD7
IL7R
LDHB
KLF2
CLEC2B
GZMA
CD63
ALOX5AP
-log10 adjusted p-value
Average Log2 Fold Change

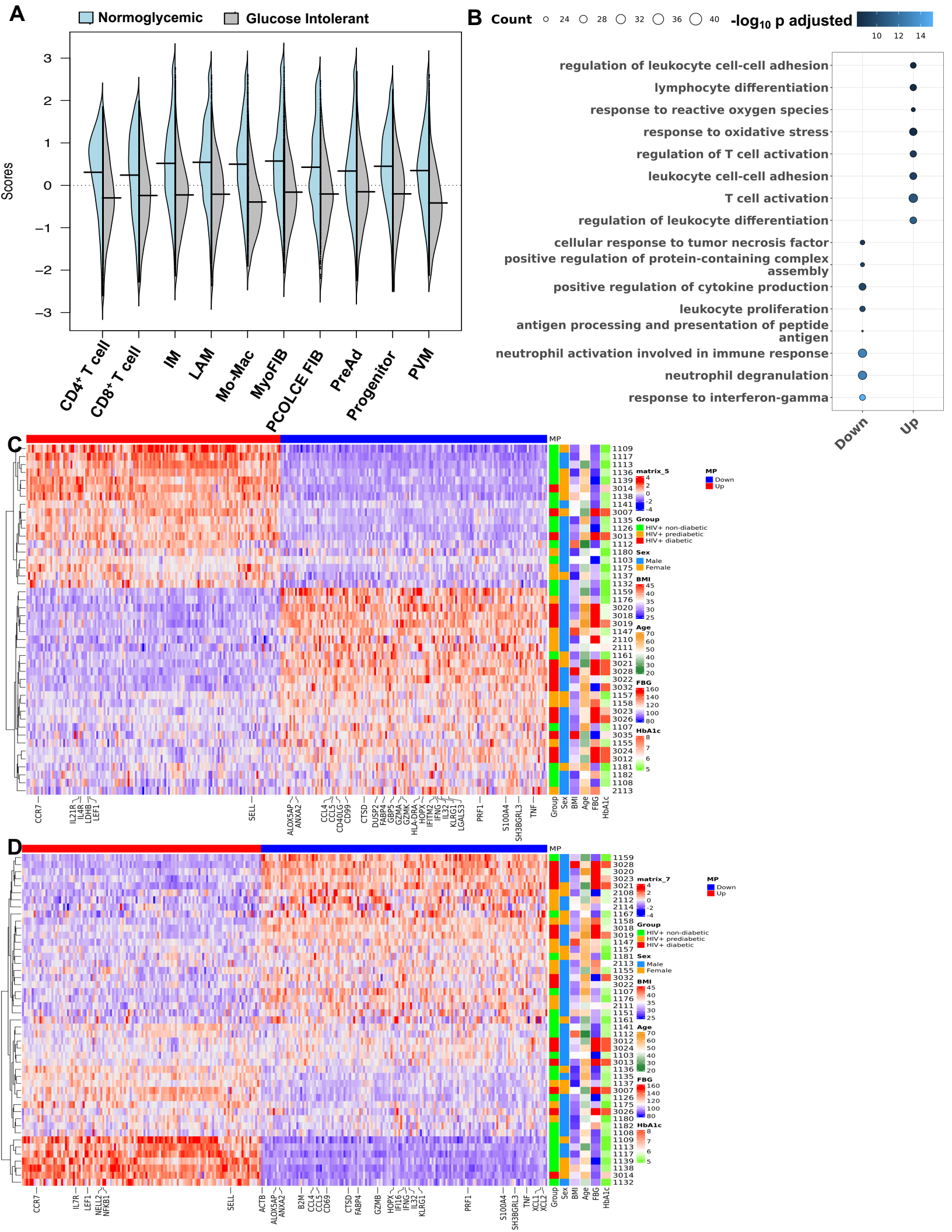
A
Normoglycemic
Glucose Intolerant
Scores
3
2
1
0
−1
−2
−3
CD4+ T cell
CD8+ T cell
IM
LAM
Mo-Mac
MyoFIB
PCOLCE FIB
PreAd
Progenitor
PVM
B
Count
24
28
32
36
40
-log10 p adjusted
10
12
14
regulation of leukocyte cell-cell adhesion
lymphocyte differentiation
response to reactive oxygen species
response to oxidative stress
regulation of T cell activation
leukocyte cell-cell adhesion
T cell activation
regulation of leukocyte differentiation
cellular response to tumor necrosis factor
positive regulation of protein-containing complex assembly
positive regulation of cytokine production
leukocyte proliferation
antigen processing and presentation of peptide antigen
neutrophil activation involved in immune response
neutrophil degranulation
response to interferon-gamma
Down
Up
C
MP
matrix_5
Group
HIV+ non-diabetic
HIV+ prediabetic
HIV+ diabetic
Sex
Male
Female
BMI
Age
FBG
HbA1c
Down
Up
CCR7
IL21R
IL4R
LDHB
LEF1
SELL
ALOX5AP
ANXA2
CCL4
CCL5
CD40LG
CD99
CTSD
DUSP2
FABP4
GBP5
GZMA
GZMK
HLA-DRA
HOPX
IFITM2
IFNG
IL32
KLRG1
LGALS3
PRF1
S100A4
SH3BGRL3
TNF
Group
Sex
BMI
Age
FBG
HbA1c
D
MP
matrix_7
Group
HIV+ non-diabetic
HIV+ prediabetic
HIV+ diabetic
Sex
Male
Female
BMI
Age
FBG
HbA1c
Down
Up
CCR7
IL7R
LEF1
NELL2
NFKB1
SELL
ACTB
ALOX5AP
ANXA2
B2M
CCL4
CCL5
CD69
CTSD
FABP4
GZMB
HOPX
IFI16
IFNG
IL32
KLRG1
PRF1
S100A4
SH3BGRL3
TNF
XCL1
XCL2
Group
Sex
BMI
Age
FBG
HbA1c

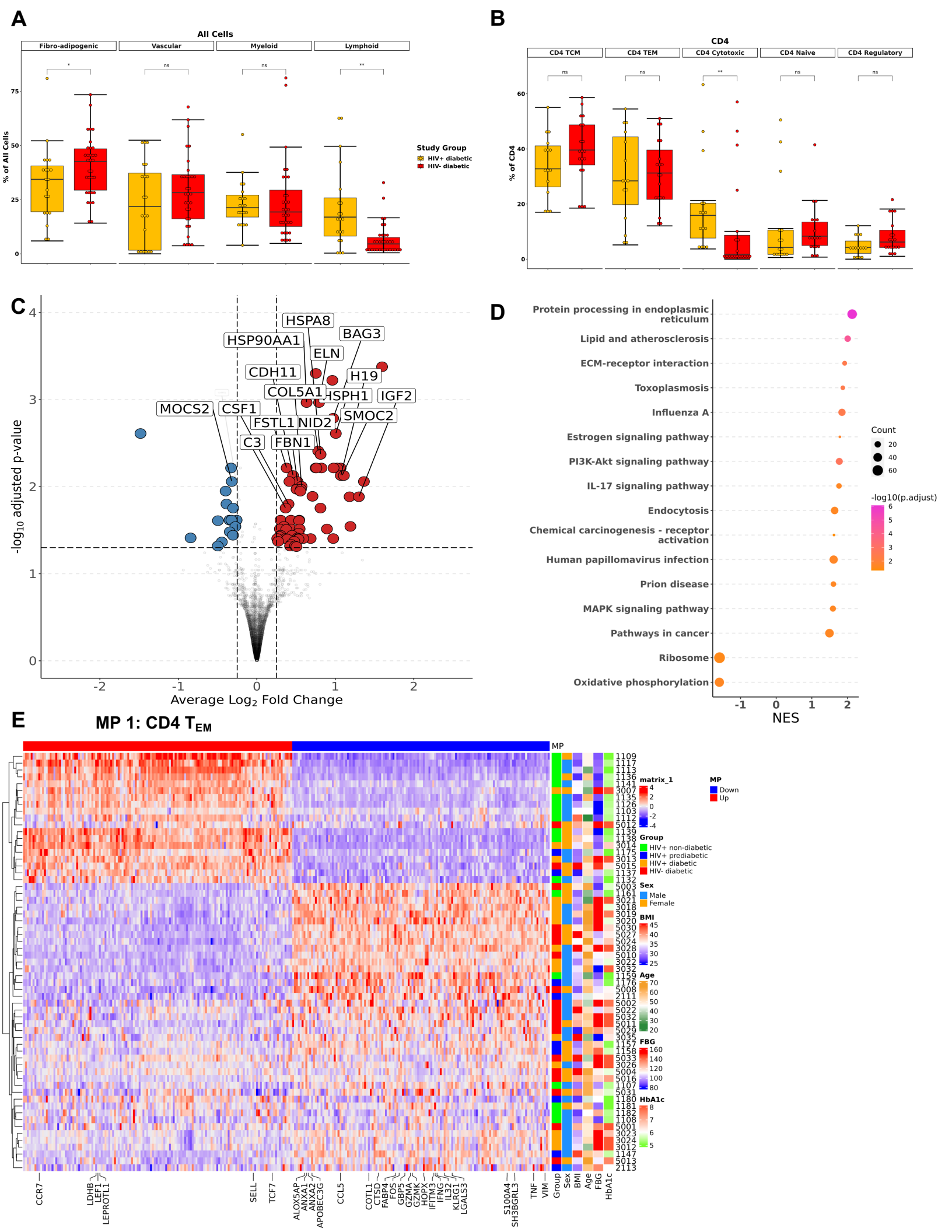
A
All Cells
Fibro-adipogenic
Vascular
Myeloid
Lymphoid
% of All Cells
Study Group
HIV+ diabetic
HIV- diabetic
B
CD4
CD4 TCM
CD4 TEM
CD4 Cytotoxic
CD4 Naive
CD4 Regulatory
% of CD4
C
HSPA8
HSP90AA1
BAG3
ELN
CDH11
H19
COL5A1
HSPH1
IGF2
MOCS2
CSF1
SMOC2
FSTL1
NID2
C3
FBN1
-log10 adjusted p-value
Average Log2 Fold Change
D
Protein processing in endoplasmic reticulum
Lipid and atherosclerosis
ECM-receptor interaction
Toxoplasmosis
Influenza A
Estrogen signaling pathway
PI3K-Akt signaling pathway
IL-17 signaling pathway
Endocytosis
Chemical carcinogenesis - receptor activation
Human papillomavirus infection
Prion disease
MAPK signaling pathway
Pathways in cancer
Ribosome
Oxidative phosphorylation
Count
-log10(p.adjust)
NES
E
MP 1: CD4 TEM
MP
Down
Up
matrix_1
Group
HIV+ non-diabetic
HIV+ prediabetic
HIV+ diabetic
HIV- diabetic
Sex
Male
Female
BMI
Age
FBG
HbA1c
CCR7
LDHB
LEF1
LEPROTL1
SELL
TCF7
ALOX5AP
ANXA1
ANXA2
APOBEC3G
CCL5
COTL1
CTSD
FABP4
FOS
GBP5
GZMA
GZMK
HLA-X
IFITM3
IFNG
IL32
KLRG1
LGALS3
S100A4
SH3BGRL3
TNF
VIM
Group
Sex
BMI
Age
FBG
HbA1c

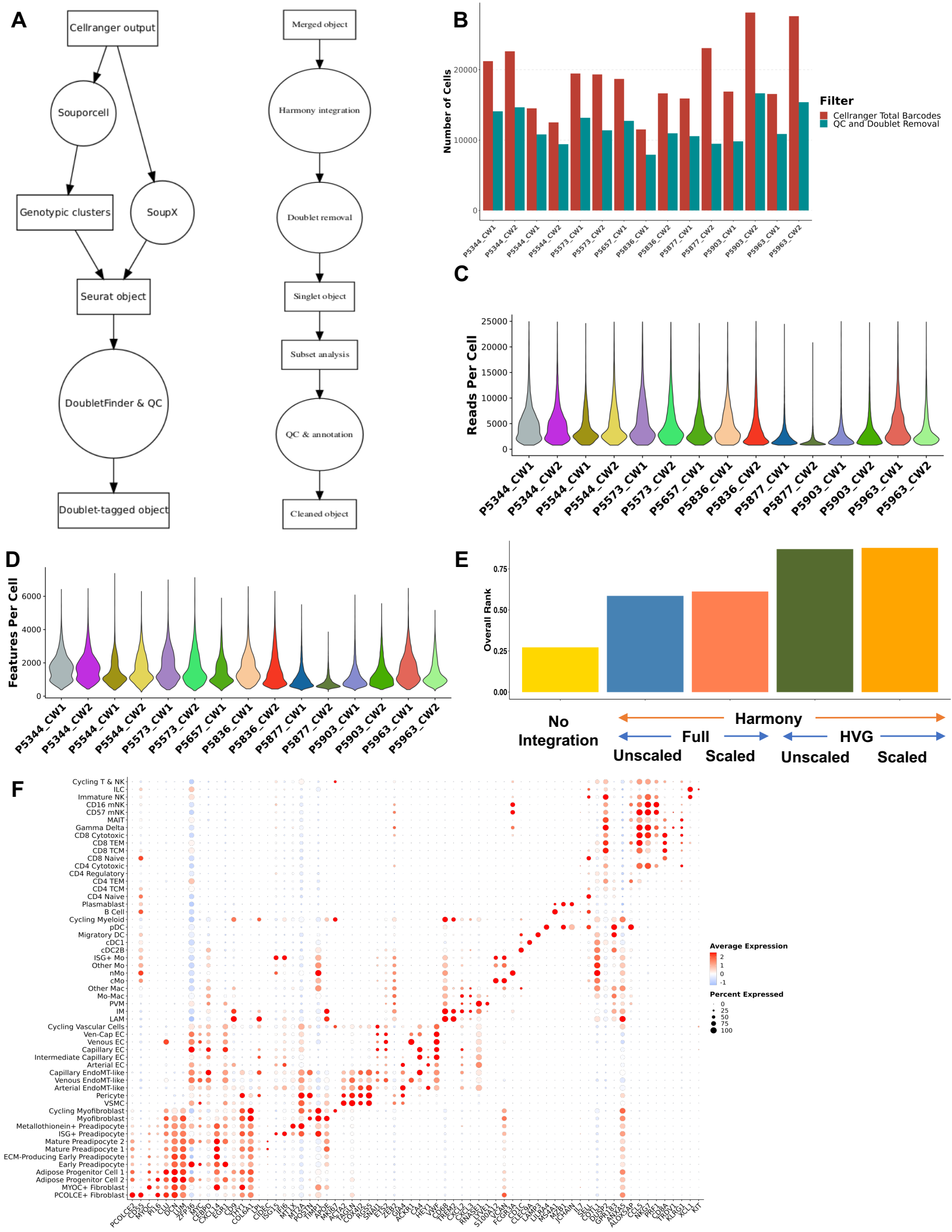
A
Cellranger output
Souporcell
Genotypic clusters
SoupX
Seurat object
DoubletFinder & QC
Doublet-tagged object
Merged object
Harmony integration
Doublet removal
Singlet object
Subset analysis
QC & annotation
Cleaned object
B
Number of Cells
Filter
Cellranger Total Barcodes
QC and Doublet Removal
C
Reads Per Cell
D
Features Per Cell
E
Overall Rank
No Integration
Harmony
Full
HVG
Unscaled
Scaled
Unscaled
Scaled
F
Average Expression
Percent Expressed

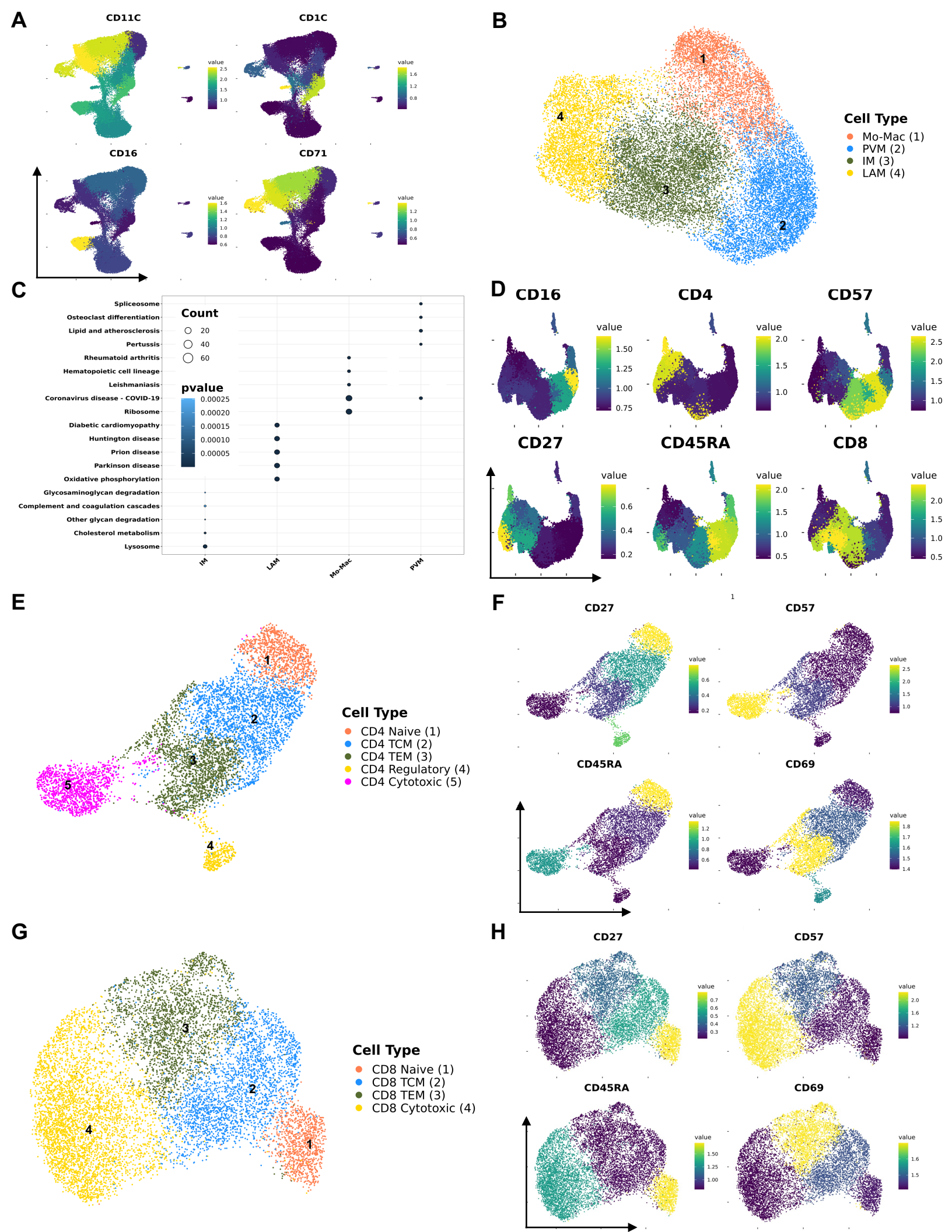
A
CD11C
CD1C
CD16
CD71
value
B
Cell Type
Mo-Mac (1)
PVM (2)
IM (3)
LAM (4)
C
Count
20
40
60
pvalue
0.00025
0.00020
0.00015
0.00010
0.00005
Spliceosome
Osteoclast differentiation
Lipid and atherosclerosis
Pertussis
Rheumatoid arthritis
Hematopoietic cell lineage
Leishmaniasis
Coronavirus disease - COVID-19
Ribosome
Diabetic cardiomyopathy
Huntington disease
Prion disease
Parkinson disease
Oxidative phosphorylation
Glycosaminoglycan degradation
Complement and coagulation cascades
Other glycan degradation
Cholesterol metabolism
Lysosome
IM
LAM
Mo-Mac
PVM
D
CD16
CD4
CD57
CD27
CD45RA
CD8
E
Cell Type
CD4 Naive (1)
CD4 TCM (2)
CD4 TEM (3)
CD4 Regulatory (4)
CD4 Cytotoxic (5)
F
CD27
CD57
CD45RA
CD69
G
Cell Type
CD8 Naive (1)
CD8 TCM (2)
CD8 TEM (3)
CD8 Cytotoxic (4)
H
CD27
CD57
CD45RA
CD69

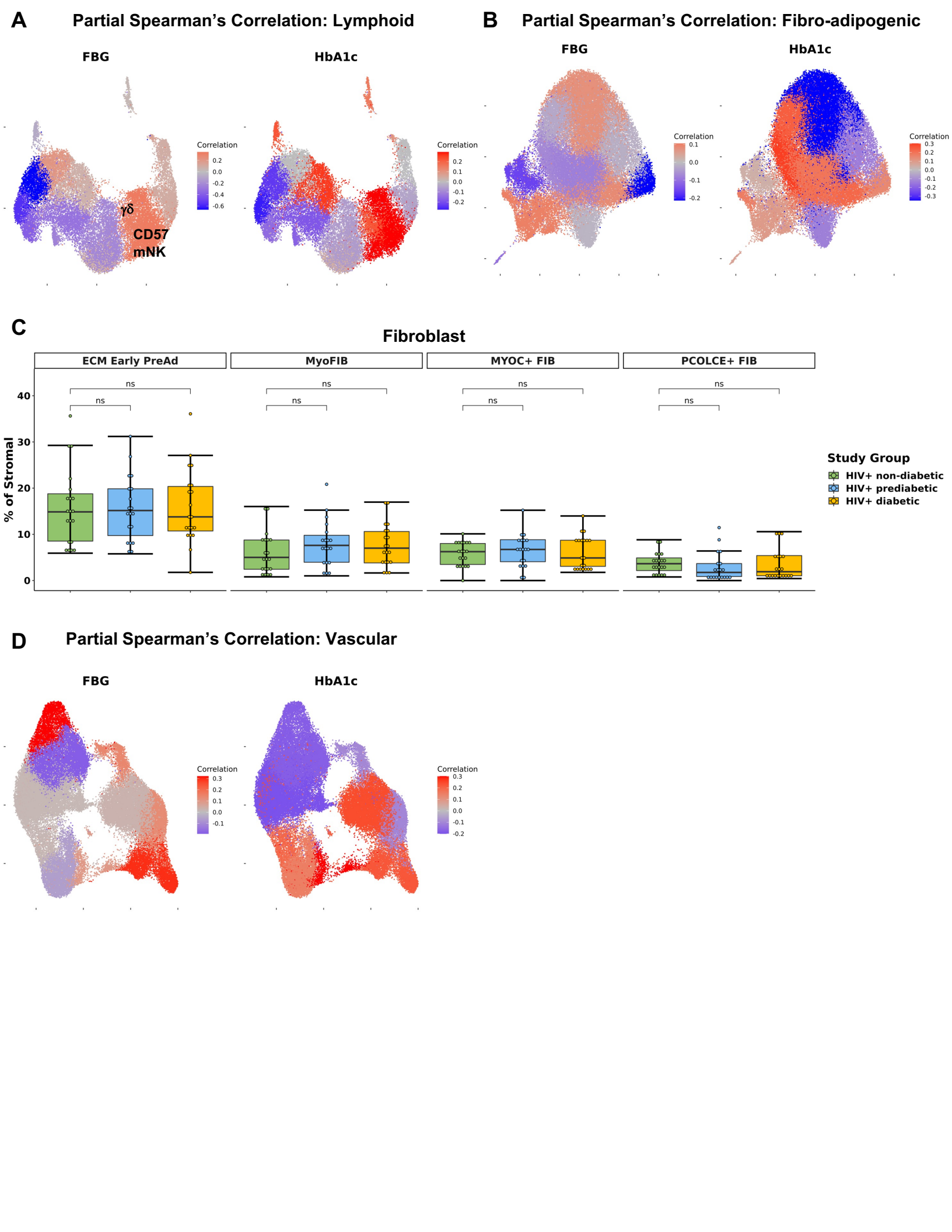
A
Partial Spearman's Correlation: Lymphoid
FBG
HbA1c
Correlation
γδ
CD57
mNK
B
Partial Spearman's Correlation: Fibro-adipogenic
FBG
HbA1c
Correlation
C
Fibroblast
ECM Early PreAd
MyoFIB
MYOC+ FIB
PCOLCE+ FIB
ns
% of Stromal
Study Group
HIV+ non-diabetic
HIV+ prediabetic
HIV+ diabetic
D
Partial Spearman's Correlation: Vascular
FBG
HbA1c
Correlation

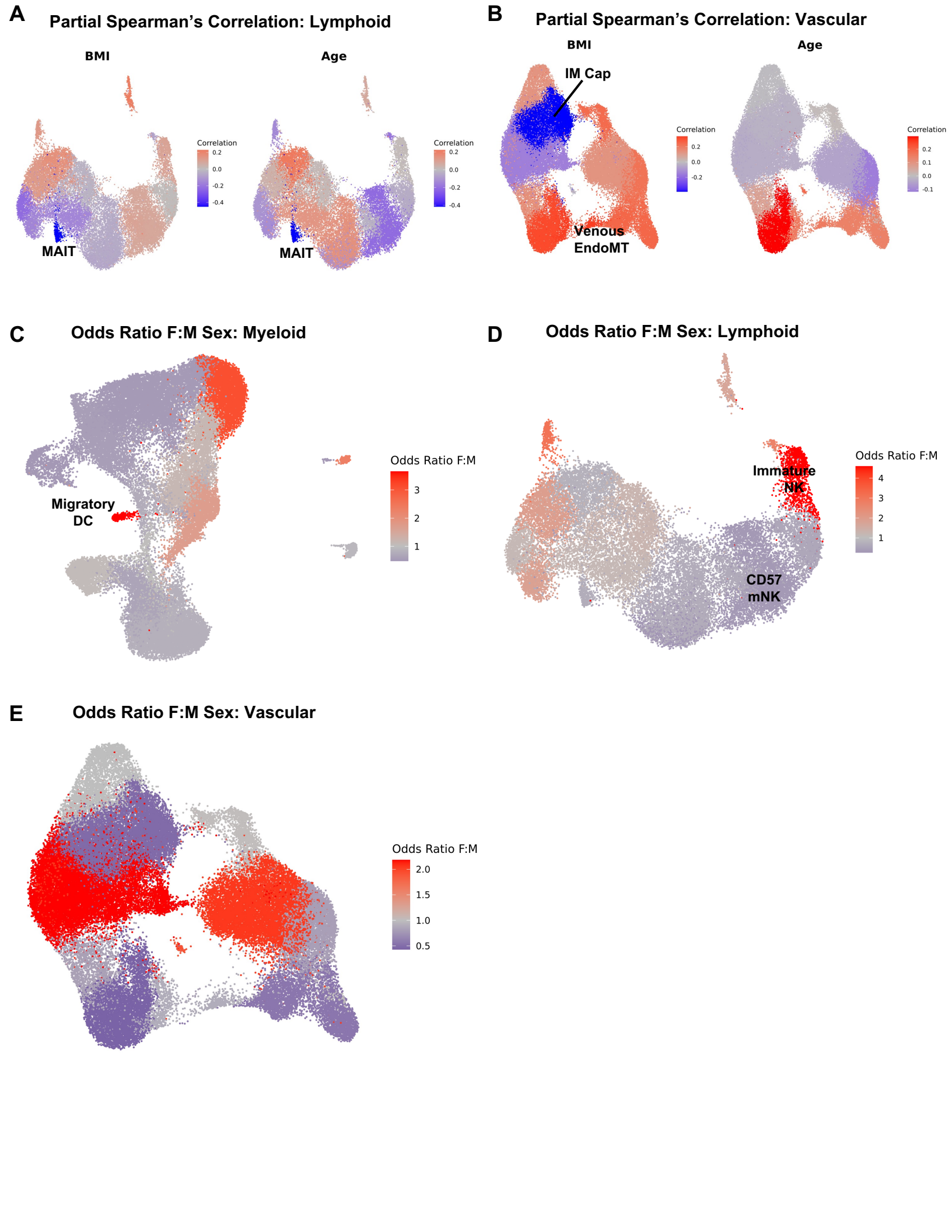
A
Partial Spearman's Correlation: Lymphoid
BMI
Age
Correlation
0.2
0.0
-0.2
-0.4
MAIT
MAIT
B
Partial Spearman's Correlation: Vascular
BMI
Age
IM Cap
Venous
EndoMT
Correlation
0.2
0.0
-0.2
0.2
0.1
0.0
-0.1
C
Odds Ratio F:M Sex: Myeloid
Migratory
DC
Odds Ratio F:M
3
2
1
D
Odds Ratio F:M Sex: Lymphoid
Immature
NK
CD57
mNK
Odds Ratio F:M
4
3
2
1
E
Odds Ratio F:M Sex: Vascular
Odds Ratio F:M
2.0
1.5
1.0
0.5

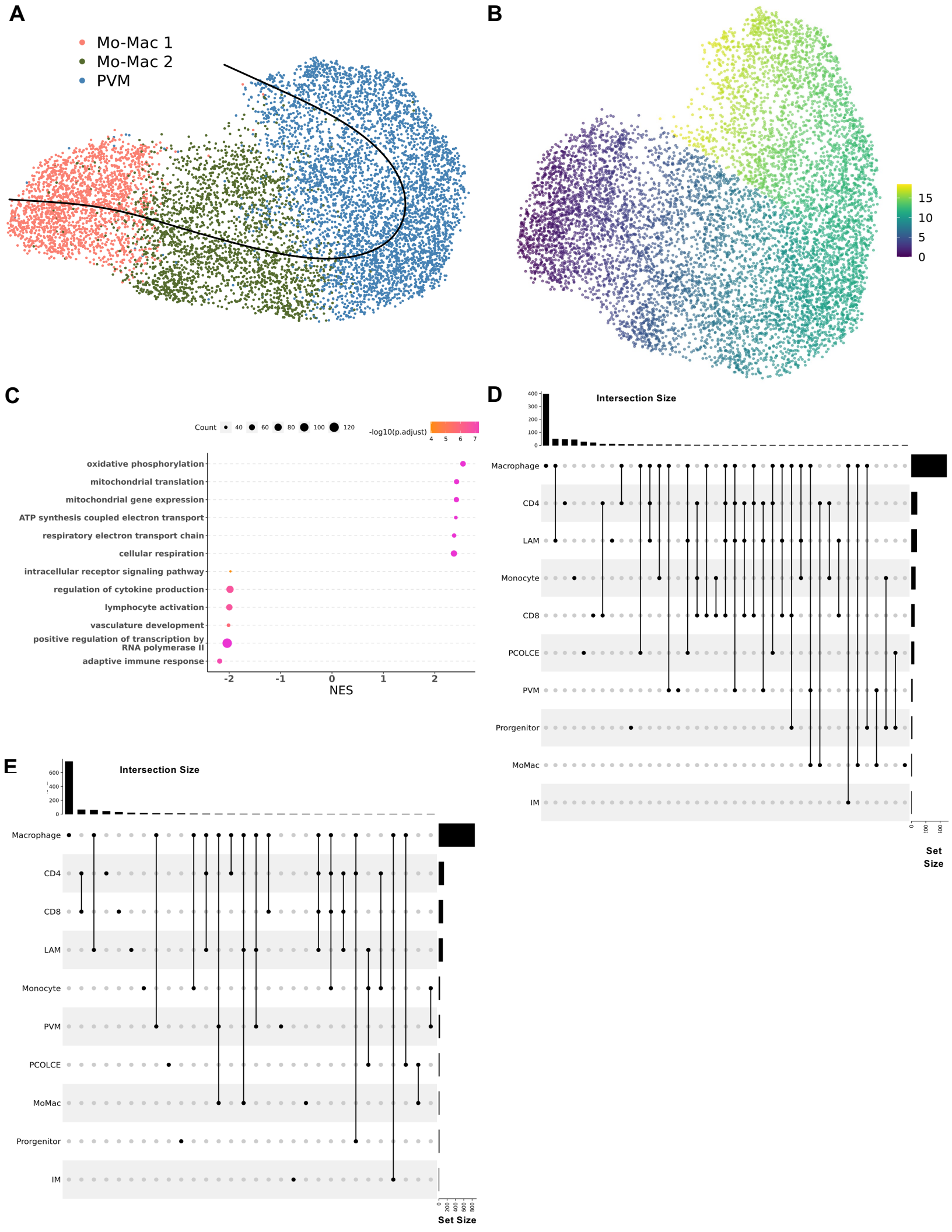
A
Mo-Mac 1
Mo-Mac 2
PVM
B
15
10
5
0
C
Count
40
60
80
100
120
-log10(p.adjust)
4
5
6
7
oxidative phosphorylation
mitochondrial translation
mitochondrial gene expression
ATP synthesis coupled electron transport
respiratory electron transport chain
cellular respiration
intracellular receptor signaling pathway
regulation of cytokine production
lymphocyte activation
vasculature development
positive regulation of transcription by RNA polymerase II
adaptive immune response
-2
-1
0
1
2
NES
D
Intersection Size
400
300
200
100
0
Macrophage
CD4
LAM
Monocyte
CD8
PCOLCE
PVM
Prorgenitor
MoMac
IM
Set Size
E
Intersection Size
600
400
200
0
Macrophage
CD4
CD8
LAM
Monocyte
PVM
PCOLCE
MoMac
Prorgenitor
IM
0
200
400
600
800
Set Size

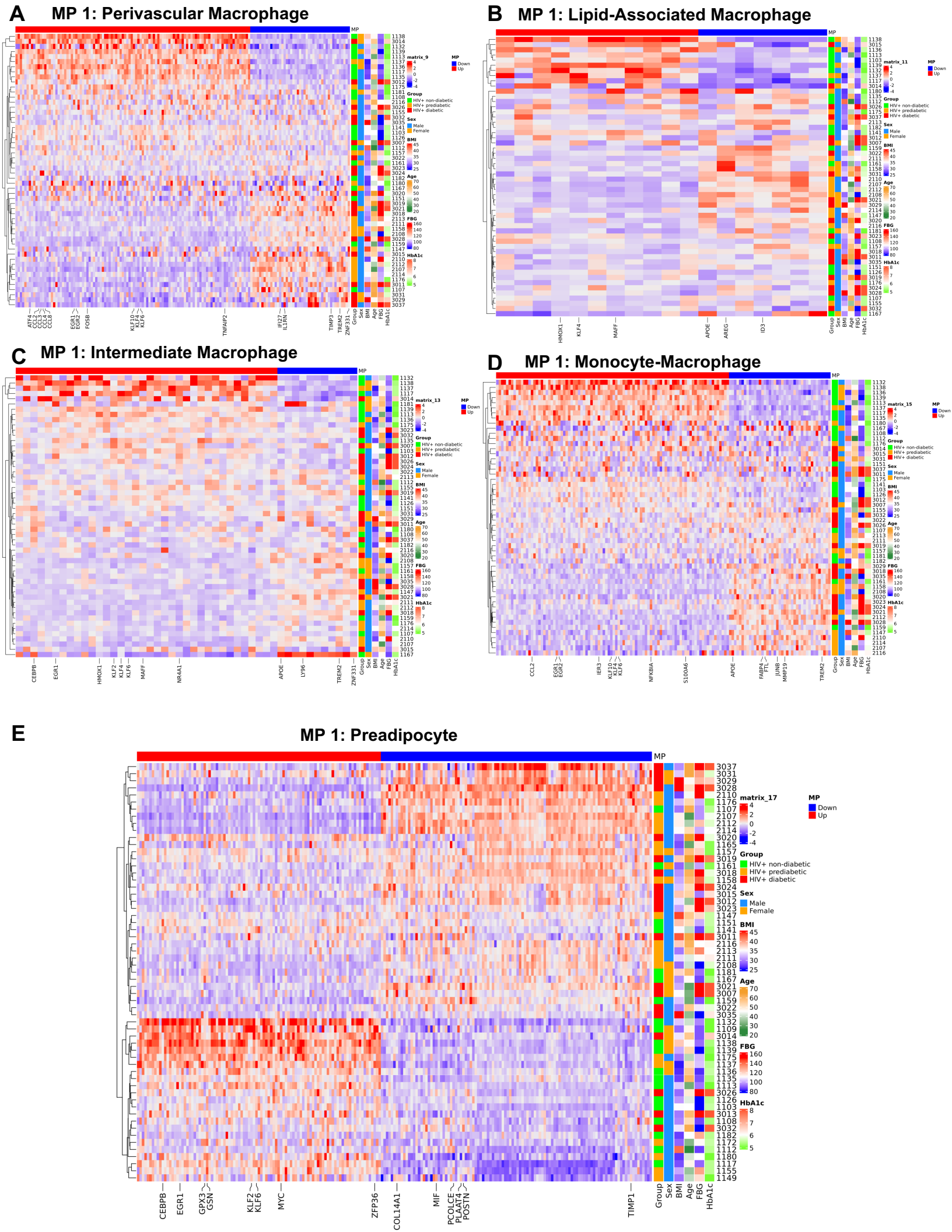
A
MP 1: Perivascular Macrophage
B
MP 1: Lipid-Associated Macrophage
C
MP 1: Intermediate Macrophage
D
MP 1: Monocyte-Macrophage
E
MP 1: Preadipocyte
MP
Down
Up
matrix_9
matrix_11
matrix_13
matrix_15
matrix_17
Group
HIV+ non-diabetic
HIV+ prediabetic
HIV+ diabetic
Sex
Male
Female
BMI
Age
FBG
HbA1c
ATF4
CCL2
CCL4
CCL4L2
CCL8
EGR1
EGR2
FOSB
KLF10
KLF4
KLF6
TNFAIP2
IFI27
ILZRN
TIMP3
TREM2
ZNF331
HMOX1
MAFF
APOE
AREG
ID3
CEBPB
NR4A1
LY96
NFKBIA
S100A6
FABP4
FTL
JUNB
MMP19
GPX3
GSN
MYC
ZFP36
COL14A1
MIF
PCOLCE
PLAAT4
POSTN
TIMP1